

Dear Dr. Topping,

October 9<sup>th</sup>, 2014

Please find attached our detailed point-by-point response to all comments by the three referees, a list of changes, and in addition a revised version of the manuscript with all changes highlighted in red. We hope that our manuscript now meets with your approval.

Yours sincerely, and on behalf of my co-authors,

Thomas Berkemeier  
Max Planck Institute for Chemistry  
Multiphase Chemistry Department  
D-55128 Mainz, Germany  
[t.berkemeier@mpic.de](mailto:t.berkemeier@mpic.de)

## Author comment to anonymous referee #1

### Referee comment 1:

Recently researchers have suggested that glassy secondary organic aerosols can cause ice nucleation. However, it is still not clear if these particles act as ice nuclei under atmospheric conditions because the processes involved are numerous and complex. In this manuscript the authors have come up with an elegant way to model these processes. Confidence in the modelling approach was gained by comparing model results with recent laboratory results. Then, model results were used to predict atmospheric conditions that may lead to ice nucleation by glassy secondary organic aerosols. The paper represents a substantial contribution to scientific progress on the topic. I expect this study will motivate future laboratory studies to constrain better some of the physical parameters needed for modelling ice nucleation on glassy secondary organic aerosols. I highly recommend this paper for publication in ACP after the authors have adequately addressed the following comments.

### Response:

*We thank anonymous referee #1 for her/his very careful study of the manuscript and we are pleased about the very positive evaluation. We will address all the comments and helpful suggestions in the revised version of the manuscript. We will clarify especially the presentation of uncertainties in the model calculations and discuss how they relate to uncertainties in model input. The very detailed specific and technical comments are highly appreciated and will all be implemented upon revision. In the following, we list point-by-point responses to the referee's comments.*

### Referee comment 2:

General comments regarding uncertainties in the calculations: Figure S4 shows FDRH of four different SOA precursors as well as their quasiequilibrium glass transition, with uncertainties represented by shaded bands. For clarity and ease of reading, it would be helpful to state in the figure caption the source of the uncertainties (i.e. what uncertainties are considered in the figure). I assume the uncertainties come from uncertainties in  $T_{g,org}$ ,  $k_{GT}$  and  $\kappa_{org}$ . Two sets of uncertainties are reported in the manuscript. The first set (shown in Figure S4) uses  $k_{GT} = 2.5 \pm 1$ . The second set of uncertainties (shown in Figure S6, orange shaded) includes a wider range of  $k_{GT}$ . From the document I could not tell which set of uncertainties is most applicable to the present modelling studies. Please clearly discuss which set of uncertainties is most applicable to the present modelling study and justify. This may have been discussed in Koop (2011), but additional discussion in the current manuscript would be very helpful.

There are large uncertainties in calculated FDRH when all the parameters are taken into account (see Figure S6). These uncertainties should be mentioned in the conclusions and perhaps the abstract. In addition, it may be helpful to the community if the authors gave some directions on measurements that are needed to help reduce the uncertainties.

### Response:

*This is correct, the uncertainties in Fig. S4 come from input parameter uncertainty. We admit that our discussion of model output uncertainty might have been confusing. Fig. S4 and Fig. S6 both use the respective input parameter uncertainties indicated in Table A1. While Fig. S4 shows the comparably small uncertainties within a certain SOA class, Fig. S6 shows the overall uncertainty that arises when using the very broad SOA 'best guess' in Koop et al. (2011). This 'best guess' did not distinguish and resolve the*

various precursor types. Figure S6 was thought to highlight which changes are induced by which input parameter. We agree that this was somewhat confusing and not well described. We will add proper references to Table A1 and an improved description to the caption of Fig. S4. Furthermore, we have completely redesigned Fig. S6.

We added a new section 3.4 to the manuscript describes the uncertainties associated with model input. In this section we also give directions on future laboratory measurements.

Referee comment 3:

Page 16473, line 15-20. If the uncertainties in the model predictions are considered, are the freezing results above 230 K still inconsistent with the model predictions?

*Response:*

*If the uncertainties in the model predictions are considered, a few of the data points can be explained, but the majority cannot, they significantly lie outside the predicted FDRH range. In fact, the sensitivity of FDRH to all model input parameters ( $T_g$ ,  $k_{GT}$ ,  $\kappa_{org}$ ) becomes very low when FDRH approaches water saturation. At a certain point, it is not possible to further lift FDRH towards the water saturation line anymore since the curvature of the  $a_w$  curve is very steep there (composition of the deliquesced shell changes quickly with increasing RH, thereby increasing the diffusion gradient of water). We will add a sentence to Sect. B2 that discusses a potential reason for the deviation between model and experiment:*

*“Possibly, insoluble products from Naphthalene OH oxidation remained solid in the otherwise fully deliquesced particle and nucleated ice heterogeneously with lower efficiency. Such a process is not considered in the model, which does not resolve single compounds and treats Naphthalene SOA as homogeneous mixture at all times.”*

Referee comment 4:

Other general comments: Page 16461, line 20-25. Full deliquescence relative humidity (FDRH) is defined as the point where the entire particle is homogeneously mixed and its water activity corresponds to that of a liquid (i.e. it is larger than that of the quasi-equilibrium glass transition). Why is the constraint of “entirely homogeneously mixed” needed? I can image a case where the water activity corresponds to a liquid everywhere in the particle, but the particle is still not homogeneously mixed due to slow diffusion in the liquid. Does this situation ever arise?

*Response:*

*This situation indeed arises in the simulations when the trajectory starts slightly above the nominal glass transition (e.g. 229 K for sucrose particles). At model runs with these starting temperatures, all features of the kinetically limited deliquescence of a glassy particle can be observed even though the particle is formally non-glassy (sharp water diffusion front, etc.).*

Referee comment 4:

Specific comments: Page 16461, line 5: I believe it should be “from” instead of “form”

*Response:*

*This will be changed in the revised manuscript.*

Referee comment 5:

For alpha-pinene are the authors using proxies corresponding to ozonolysis or OH oxidation. Please specify for clarity.

*Response:*

*The model studies we referred to were simulating  $\alpha$ -pinene SOA from dark ozonolysis (Shilling et al., 2009; Zuend and Seinfeld, 2012). The substances found in field measurements (MBTCA, terpenylic acids) could be formed by either photooxidation and ozonolysis. This was clarified in Sect. A2, which now reads:*

*The group “ $\alpha$ -Pinene” contains compounds characteristic for photooxidation and ozonolysis of the biogenic SOA precursor  $\alpha$ -pinene, which has been chosen as proxy for the different monoterpene VOCs responsible for biogenic SOA formation.*

Referee comment 6:

Page 16462, “Ice nucleation regimes”: Through the section, please reference the updraft velocity and the corresponding type of clouds, when possible (e.g. at page 16462, line 19).

*Response:*

*We will reference the paper of Jensen et al., ACP (2005) at all three instances in the revised version of the manuscript.*

Referee comment 7:

Page 16467, line 14: Should “latitude” be replaced with “altitude”.

*Response:*

*This will be changed in the revised manuscript*

Referee comment 8:

Figures: All figures. Please indicate what size of droplets the homogeneous freezing line corresponds to.

*Response:*

*The homogeneous freezing line is a model result as described in Sect. 2. As particles increase in size during the humidification process, the size of the droplets at the homogeneous freezing line is not a constant. In Fig. 2B and Fig. 3A, this would lead to multiple hom. freezing lines that are undistinguishably close. For these two figure panels we used the homogeneous freezing line obtained for 100 nm sucrose particles, humidified at a rate of 1 % RH min<sup>-1</sup>. Since in these figures the hom. freezing line functions only as a reference point and the induced error is very small, we decided to not dwell on this simplification in the figure caption.*

Referee comment 9:

Figure 1 caption: I believe there is a typo for “typical”.

*Response:*

*This will be changed in the revised manuscript*

Referee comment 10:

Supplement: Table S1, column 1. References are not properly formatted. For example see “Kautzman 122”. Also there is some nomenclature in this column that is not defined. For example what does “CARB” represent.

*Response:*

*We apologize for the inconsistent nomenclature in Table S1. We tried to adopt most compound names from the original publications. We will clarify this with a number of additional footnotes explaining the origin of the specific compound name.*

Referee comment 11:

I can't see Table S3 mentioned anywhere in the text (either main text or supplemental). Please discuss somewhere how these parameters are used.

*Response:*

*The reference in I.54 was erroneously pointing toward Fig. S2, but should have pointed toward Fig. S3. This will be changed in the revised manuscript.*

Referee comment 12:

Line 52: (“cf figure”) give a number to the figure if possible.

*Response:*

*We will include the reference to Figure B2 in the revised manuscript.*

Referee comment 13:

The caption of Table S2 does not appear to be consistent with the data in the table.

*Response:*

*We hope we can resolve the confusion by redirecting the earlier mentioned reference from Table S2 to Table S3 (see response to comment 11).*

## Author comment to anonymous referee #2

Referee comment 1:

Organic aerosols are prevalent in the atmosphere, but little is known about their impact on ice nucleation. The paper presented here modeled the phase transitions of model organic aerosols representing both anthropogenic and biogenic SOA due to updrafts in clouds. The phase transitions for each organic aerosol were used to predict the ice nucleation regime the particle would be involved in (deposition, immersion, homogenous) and at which temperature and RH. The novel approach and results presented in this paper will greatly help in modeling ice nucleation due to organic aerosols in cirrus and other high altitude clouds. Future studies including other organics will be interesting and are necessary to assess the magnitude of the impact of organic aerosols on IN globally. This paper does a good job of visualizing the competing effects of aging (increased hygroscopicity and increased temp of glass transition) and the concepts presented. The schematics were very helpful and informative. I recommend this paper for publication.

*Response:*

*We thank anonymous referee #2 for her/his positive review of the article and appreciate the suggestions she/he made to further improve the quality of the paper. We will include changes towards all comments in the revised version of the manuscript as detailed below.*

Referee comment 2:

General Comments: The stated temperature range where glassy aerosols would be important for ice nucleation is in the range of homogeneous ice nucleation. Therefore, how important globally do you think these organic aerosols are? There is some discussion of impacts at the end of the paper, but more discussion on this temperature range and impacts would make the paper stronger. Do the authors have any suggestions for other types of organic aerosols that should be modeled next? Or predications for which organic aerosol types are most important for ice nucleation globally or in certain regions?

*Response:*

*We see our work as an explorative microphysical modelling study which describes and quantifies the different ice nucleation regimes of organic aerosols for the first time. It is less focused on the global consequences of these mechanisms. While such a study would be very worthwhile, we think quick implications are difficult to draw and an in-depth discussion would be outside the scope of our paper. In Sect. 4, we already point out that aerosol particles originating from aromatic precursors and highly aged particles derived from monoterpenes have the highest potential to affect ice cloud properties. Despite the fact that aromatic SOA particles might be produced predominantly in the exhaust plumes of urban and industrial areas, it is hard to confine their range of ice nucleation activity to certain regions due to their long lifetime in the atmosphere. The global impact is also hard to estimate, for many different reasons. Not only are the thermodynamic input parameters for our microphysical model (such as diffusivities) still subject to large uncertainties, but also is the actual microphysical process of ice nucleation on glassy particles still little understood, which is reflected in the huge spread of experimentally determined ice nucleation onsets that vary strongly between different investigated substances and experimental techniques. We would like to refer to the discussion of this issue in the revised manuscript, see also author comment to anonymous referee #3.*

Referee comment 3:

Specific Comments: Page 16454 Lines 8-9: "low temperature and low humidity" Please specify the range of temperature and humidity or add < XX \_C, < XX % RH for more clarity.

*Response:*

*Since glass temperature and glass relative humidity are interconnected, we decided to add exemplary glass transitions temperatures for two values of relative humidity that can be encountered in the atmosphere. We will add the following sentence:*

*"For example, typical  $\alpha$ -pinene derived secondary organic aerosol particles are expected to be in a glassy state below about 260 K at 30 % relative humidity, whereas at a higher humidity of 80 %, such glass transition is expected at approximately 215 K (Koop et al., 2011)."*

Referee comment 4:

Page 16460 Lines 25-26: The definition of RHg is given, but as written it was confusing. Perhaps write "The quasi-equilibrium glass transition of the aqueous organic, RHg, is shown in grey." or similar.

*Response:*

*We accept the suggestion of the referee and will change the sentence accordingly.*

Referee comment 5:

Page 16461: Figure 1 and the discussion of it in the text may benefit from labeling the circles as ABCD or 1234 and referring to them in the text by the number or letter for more clarity and less wordiness in the discussion.

*Response:*

*We agree that the figure would benefit from further labeling. We will assign labels (1234) to the four depicted particles and refer to these from the main text in the following way:*

*"Several morphological stages can be distinguished during the humidification process in Fig. 1. Starting from a homogeneous, glassy particle (1), an increase in RH first leads to liquefaction of a thin outer layer and emergence of a core-shell morphology (2). This liquid outer layer grows in equilibrium with ambient relative humidity and also extends towards the particle centre by diffusion of water into the glassy organic matrix (3), leading to shrinkage of the residual glassy core until the particle is fully deliquesced (4)."*

Referee comment 6:

Page 16463: A little more discussion of the Baustian 2013 data and how it relates to the model in the text, not only in the appendix, would be beneficial to the reader.

*Response:*

*We agree with the referee and will add the following sentences to Sect. 3.2:*

*“Baustian et al. used optical microscopy in conjunction with a cold stage to detect ice nucleation on glassy sucrose particles (4  $\mu\text{m}$  diameter) during humidification (1 % RH  $\text{min}^{-1}$ ), leading to the nucleation onsets shown in Fig. 2C (brown markers). A range of simulations mimicking the experimental conditions at different starting temperatures leads to a continuous FDRH curve (solid blue line) over the entire temperature range. For details on the calculations see Appendix B.”*

Referee comment 7:

Figure 1 caption: The specific time scale should be added either on the schematic or at the end of the last sentence in the caption, where it is mentioned.

*Response:*

*We will add the typical time scale for atmospheric updrafts to the caption of Figure 1. The respective sentence now reads:*

*“The speed of the displayed trajectory corresponds to that typical for cloud chamber or environmental cell experiments (0.1 - 1.5 K  $\text{min}^{-1}$ , 1 - 15 % RH  $\text{min}^{-1}$ )”.*

### Author comment to anonymous referee #3

Referee comment 1:

First of all, I am very sorry for the delay with sending these comments. This paper presents model calculations and conceptual analysis of the competing effects of particulate phase diffusion vs. ice nucleation, commenting on the ways that organic aerosols can interact with clouds. The paper makes useful points and is probably a good starting point for further studies, although a lot needs to be done still to resolve the different processes through which organic aerosols interact with clouds. I think this paper can be considered for publication in ACP once the following points, along with the points raised by the other reviewers, have been addressed by the authors.

*Response:*

*We gratefully thank anonymous referee #3 for her/his review of our manuscript and appreciate the suggestions she/he made to improve the quality of the paper. In the following, we will address the comments individually.*

Referee comment 2:

Major/general comments:

1. If I understand correctly, you assume constant hygroscopicity parameter for your mixtures. As you probably know, however, the hygroscopicity parameter depends on the RH/supersaturation in case the organic material is not completely dissolved. Now the authors limit the discussion in the main paper to kinetic transport vs. ice nucleation, while the organic solubility is not discussed at all. I think the authors should add a discussion on how the solubility of organic compounds and its dependence on external conditions (water content, temperature) would affect the results / play into the conceptual scheme.

*Response:*

*The model calculations in this study assume that water and oxidized organics are perfectly miscible over the observed humidity range (55 – 95 % RH). For the model system sucrose, which is described first in this paper, this assumption certainly holds and also a full, multi-parameter water activity parameterization has been used to describe sucrose hygroscopicity. For simplification of the very complex system of secondary organic aerosol (SOA), water activity of SOA is parameterized using a constant hygroscopicity parameter  $\kappa_{org}$ . We note that  $\kappa_{org}$  is not well known at these low temperatures, which is why we neglected a composition/RH dependence of it. While this is certainly not a perfect description of such a complex system, we think that the generality of our approach (SOA mixtures are derived from marker substances bundled into classes of same precursor origin) justifies the use of such a rather simple measure. A recent paper by You and Bertram (Atmos. Chem. Phys. Discuss., 2014) did not observe any temperature dependence of liquid-liquid phase separation, suggesting no major changes in the thermodynamic solution properties of those organics.*

*To clarify the origin of our hygroscopicity estimates, we added a clarifying sentence to section 3.3, which reads as follows:*

*“Hygroscopicities of the various SOA were taken from Lambe et al. (2011), who suggested that  $\kappa_{org}$  can be parameterized independently of SOA type as function of O/C ratio.”*

*In fact, in our modelling studies, uncertainty in  $\kappa_{org}$  is among the stronger uncertainties, which will be evident from a new Fig S6. Moreover, we add a subsection on limitations and uncertainties of the model to section 3 of the manuscript that addresses the problem of uncertain thermodynamic parameters.*

*While a measured  $\kappa_{org}$  value in principle considers insoluble fractions, the model does not resolve them numerically and doesn't assign ice nucleation activity to them. To clarify this point we added the following sentence to the discussion in Sect. B2:*

*"Possibly, insoluble products from Naphthalene OH oxidation remained solid in the otherwise fully deliquesced particle and nucleated ice heterogeneously with lower efficiency. Such a process is not considered the model, which does not resolve single compounds and treats Naphthalene SOA as homogeneous mixture at all times."*

Referee comment 3:

2. Besides the solubility, another thermodynamic parameter that is likely to be strongly influenced by the water content as well as temperature is the volatility of the organic material. I think this too deserves some discussion on the paper. This paper seems to focus on the importance of the phase state on the kinetics of water in the organic matrix, but I think the importance of the phase state for the energetics/thermodynamics of the organic system (manifested in solubility and equilibrium vapour pressures) deserve some discussion as well.

*Response:*

*In this study, we looked at organic aerosol under cirrus conditions, i.e. at temperatures below 240 K. While volatility plays an important role in gas-to-particle partitioning of SOA in general, volatilization of organic compounds is expected not to be significant during our model simulations under these low temperature conditions. We thus find it reasonable to neglect volatilization effects for our study. We have added this information to the new section 3.4:*

*"Volatilization of organic material has not been included in the calculations presented above since vapour pressures of typical SOA marker compounds are low under the low temperature conditions employed in this study (Huisman et al., 2013; O'Meara et al., 2014)."*

Referee comment 4:

3. I would have appreciated a discussion on the potential limitations of the model and what kind of experiments the authors would need to constrain it better.

*Response:*

*The largest uncertainty in the simulations presented in this paper arises from the uncertainty in input parameters. In particular, the model would benefit from accurate parameterizations for the water diffusion coefficient inside SOA particles. Until now, these values are practically unknown. This paper makes a first attempt to estimate diffusivities of water within such complex organic mixtures.*

*Additionally, the heterogeneous ice nucleation process on glasses needs more detailed understanding and investigations so that accurate and reliable nucleation onsets are available for a larger number of different compounds and also mixtures of these compounds.*

*We agree that such a discussion might be worthwhile and added a full section 3.4 to discuss model uncertainties to the revised version of the manuscript.*

Referee comment 5:

Minor/specific comments:

4. Abstract, p. 16452, line 20: I find the concluding statement of the abstract a bit too general and vague. Please be a bit more specific here. What kind of formalisms are needed? What would be the first, most critical, improvements in the atmospheric models that one should start with?

*Response:*

*In our opinion, atmospheric models should, after further careful studies have been conducted, implement organic aerosols as ice nuclei. This study suggests upper temperature limits below which these particles can act as ice nuclei at a certain ice supersaturation. We also show that a potential parameterization of a heterogeneous ice nucleation onset must include air parcel updraft velocity and particle size to account for the competition between water uptake and ice nucleation on these particles. We will thus add the following sentence to the abstract:*

*“For the incorporation of ice nucleation by organic aerosol particles into atmospheric models, our results demonstrate a demand for model formalisms that account for the effects of molecular diffusion and describe ice nucleation onsets not only as a function of temperature and relative humidity, but also include updraft velocity, particle size and composition.”*

## List of changes

- Edited abstract
- Edited section 1, introduction
  - o l. 54-59
  - o l. 76-79
- Small, technical changes in section 3.1
- Included references in section 3.2
- Included sentences to section 3.2, l. 311-318
- Added sentence to section 3.3, l. 332-334
- New section 3.4
- Edited section 4, l. 469-486
- Small, technical changes in appendix A2
- Added discussion on insolubilities, appendix B2
- Edited Figure 1 + caption
- Small, technical changes in Figure B1 caption
  
- Corrected two references to tables and figures in supplement text (supplement)
- Corrected Eq. S15 (supplement)
- Edited footnotes in Table S1 (supplement)
- Edited Table S3 (supplement)
- Edited Figure S4 caption (supplement)
- Newly designed Figure S6 + caption (supplement)

1 **Competition between water uptake and ice nucleation by**  
2 **glassy organic aerosol particles**

3

4 **T. Berkemeier<sup>1,2</sup>, M. Shiraiwa<sup>1</sup>, U. Pöschl<sup>1</sup> and T. Koop<sup>2,\*</sup>**

5 [1] Multiphase Chemistry Department, Max Planck Institute for Chemistry, Mainz, Germany

6 [2] Faculty of Chemistry, Bielefeld University, Bielefeld, Germany

7

8 Correspondence to: T. Koop ([thomas.koop@uni-bielefeld.de](mailto:thomas.koop@uni-bielefeld.de))

9

10 *To be submitted to Atmospheric Chemistry and Physics (ACP)*

11

12 Short title: Water uptake and ice nucleation by glassy organic aerosols

13 **Abstract**

14 Organic aerosol particles play a key role in climate by serving as nuclei for clouds and  
15 precipitation. Their sources and composition are highly variable, and their phase state ranges  
16 from liquid to solid under atmospheric conditions, affecting the pathway of activation to cloud  
17 droplets and ice crystals. Due to slow diffusion of water in the particle phase, organic  
18 particles may deviate in phase and morphology from their thermodynamic equilibrium state,  
19 hampering the prediction of their influence on cloud formation. We overcome this problem by  
20 combining a novel semi-empirical method for estimation of water diffusivity with a kinetic  
21 flux model that explicitly treats water diffusion. We estimate timescales for particle  
22 deliquescence as well as various ice nucleation pathways for a wide variety of organic  
23 substances, including secondary organic aerosol (SOA) from the oxidation of isoprene,  $\alpha$ -  
24 pinene, naphthalene, and dodecane. The simulations show that in typical atmospheric  
25 updrafts, glassy states and solid/liquid core-shell morphologies can persist for long enough  
26 that heterogeneous ice nucleation in the deposition and immersion mode can dominate over  
27 homogeneous ice nucleation. Such competition depends strongly on ambient temperature and  
28 relative humidity as well as humidification rates and particle sizes. Reflecting difference in  
29 glass transition temperature, hygroscopicity and atomic O/C ratio of SOA, naphthalene SOA  
30 particles have the highest potential to act as heterogeneous ice **nuclei**. Our findings  
31 demonstrate that kinetic limitations of water diffusion into organic aerosol particles **are likely**  
32 **to be encountered under atmospheric conditions and** can strongly affect ice nucleation  
33 pathways. For the incorporation of **ice nucleation by organic aerosol particles into**  
34 **atmospheric models, our results demonstrate a demand for model formalisms that account for**  
35 **the effects of molecular diffusion and describe ice nucleation onsets not only as a function of**  
36 **temperature and relative humidity, but also include updraft velocity, particle size and**  
37 **composition.**

## 38 1 Introduction

39 Atmospheric aerosol particles influence climate through affecting the earth's radiation budget  
40 directly by scattering and absorbing light, and indirectly by acting as nuclei for cloud droplets  
41 and ice crystals (Yu et al., 2006; Andreae and Rosenfeld, 2008; IPCC, 2013). Ice nucleation is  
42 an important pathway for high-altitude cirrus cloud formation and it occurs either  
43 homogeneously in liquid aerosol particles or heterogeneously in the presence of active ice  
44 nuclei (IN), which are solid particles that facilitate nucleation. Homogeneous ice nucleation  
45 generally requires high supersaturations in aqueous aerosol droplets, occurring at ice  
46 saturation ratios of  $S_{\text{ice}} \geq 1.4$  (Koop et al., 2000). Only a small fraction of atmospheric aerosol  
47 particles act as IN below this homogeneous ice nucleation threshold (DeMott et al., 2003;  
48 Cziczo et al., 2013). Heterogeneous ice nucleation can occur via several pathways such as  
49 deposition nucleation, i.e. deposition of gaseous water molecules to form crystalline ice on a  
50 solid IN, or immersion freezing, which describes nucleation induced by IN immersed in  
51 supercooled aqueous droplets (Pruppacher and Klett, 1997; Hoose and Möhler, 2012).

52 Organic aerosol particles are ubiquitous and abundant in the atmosphere, but traditionally are  
53 not referred to as effective IN when compared to dust or biological particles (see Hoose and  
54 Möhler (2012) and references therein). **More recently, however, several laboratory studies**  
55 **have shown that glassy organic particles can act as IN at low-temperature cirrus conditions in**  
56 **the deposition mode or at slightly elevated temperatures in the immersion mode (Murray et**  
57 **al., 2010; Wagner et al., 2012; Wang et al., 2012; Wilson et al., 2012; Baustian et al., 2013;**  
58 **Schill et al., 2014), in agreement with inferences from field data (Froyd et al., 2010; Knopf et**  
59 **al., 2010; Knopf et al., 2014). This IN ability has been observed for a number of different**  
60 **types of particles composed of pure organic substances such as simple sugars and acids**  
61 **(Murray et al., 2010; Wagner et al., 2012; Wilson et al., 2012; Baustian et al., 2013) and**  
62 **biomass burning marker compounds (Wagner et al., 2012; Wilson et al., 2012), for (phase-**  
63 **separated) organic-inorganic mixtures (Wagner et al., 2012; Wilson et al., 2012; Baustian et**  
64 **al., 2013; Schill and Tolbert, 2013), as well as for SOA particles derived from aromatic VOCs**  
65 **(Wang et al., 2012) or emerging from aqueous phase reactions (Schill et al., 2014). It has also**  
66 **been proposed recently that formation of highly porous structures upon atmospheric freeze-**  
67 **drying could enhance the IN ability of organic aerosol particles (Adler et al., 2013).**

68 These observations suggest a connection between particle phase state and the resulting  
69 predominant ice nucleation pathway (Murray et al., 2010). Organic aerosol particles can adopt

70 liquid, semisolid or solid states, or may even exhibit mixed phases, depending on composition  
71 and ambient conditions (Mikhailov et al., 2009; Koop et al., 2011; Vaden et al., 2011; Kuwata  
72 and Martin, 2012; Perraud et al., 2012; Song et al., 2012; You et al., 2012; Renbaum-Wolff et  
73 al., 2013; Kidd et al., 2014). SOA particles are expected to be liquid at high temperature and  
74 high humidity, but are very likely to exhibit a highly viscous semisolid or even glassy state at  
75 low temperature and low humidity (Virtanen et al., 2010; Saukko et al., 2012; Renbaum-  
76 Wolff et al., 2013; Shiraiwa et al., 2013a). For example, typical  $\alpha$ -pinene derived secondary  
77 organic aerosol particles are expected to be in a glassy state below about 260 K at 30 %  
78 relative humidity, whereas at a higher humidity of 80 %, such glass transition is expected at  
79 approximately 215 K (Koop et al., 2011). Glassy states are characterized by viscosities greater  
80 than  $10^{12}$  Pa s, corresponding to diffusion time scales within these particles that can exceed  
81 days or even years (Shiraiwa et al., 2011; Koop et al., 2011; Zhou et al., 2013). Water uptake  
82 into glassy aerosols has been shown to occur slowly and to proceed gradually with increasing  
83 relative humidity (Mikhailov et al., 2009; Tong et al., 2011; Zobrist et al., 2011; Bones et al.,  
84 2012; Price et al., 2014).

85 Hence, several competing processes can occur in glassy organic aerosol particles during  
86 updraft of an air parcel: Heterogeneous ice nucleation in the deposition mode onto the glassy  
87 solid aerosol surface; diffusion of water into the particle, inducing a gradual phase transition  
88 towards the liquid state; and immersion freezing during the transition between both states. In  
89 order to determine those atmospheric conditions at which one of these processes dominates,  
90 we employ a numerical aerosol diffusion model based on the kinetic multi-layer model for  
91 gas-particle interactions in aerosols and clouds (KM-GAP), which explicitly treats mass  
92 transport of water molecules in the gas and particle phases (Shiraiwa et al., 2012). Due to  
93 experimental constraints associated with very long observation times, parameterizations for  
94 water diffusivity in glassy organic material are sparse and hence are only known for a few  
95 model compounds. Therefore, water diffusivity in SOA materials from various biogenic and  
96 anthropogenic precursors are deduced from water diffusivity parameterizations of model  
97 compounds using a semi-empirical physico-chemical model of water diffusion in glass-  
98 forming aqueous organics.

99

## 100 **2 Modelling approach**

### 101 **2.1 Numerical diffusion model**

102 The numerical diffusion model employed in this study is based on the kinetic multi-layer  
103 model for gas-particle interactions in aerosols and clouds, KM-GAP (Shiraiwa et al., 2012).  
104 KM-GAP consists of multiple model compartments and layers, respectively: gas phase, near-  
105 surface gas phase, sorption layer, surface layer, near-surface bulk, and a number of  $n$  bulk  
106 layers (cf. Fig. S1 in the supplementary material). The following processes are considered in  
107 KM-GAP: gas phase diffusion, gas-surface transport, surface-bulk transport, and bulk  
108 diffusion. The bulk layers can either grow or shrink in response to mass transport. The initial  
109 bulk layer sizes are chosen small enough to ensure numerical convergence (usually 100-750  
110 layers), but are not allowed to fall below the molecular length scale ( $\sim 0.3$  nm).

111 The model was complemented by modules predicting homogeneous ice nucleation as a  
112 function of water activity according to Koop et al. (2000), heterogeneous ice nucleation at a  
113 pre-defined ice supersaturation level, and it considers Kelvin effects. Moreover, a few further  
114 conceptual changes have been introduced to the original KM-GAP, including a more explicit  
115 treatment of gas diffusion, composition-based bulk diffusion and a mechanism of surface-to-  
116 bulk transport facilitated by surface-adsorbed water, as detailed in the following sections.  
117 Parameterizations of composition-dependent density, water activity and bulk diffusivity for  
118 the sucrose/water system have been adopted from Zobrist et al. (2011). A detailed description  
119 of the gas diffusion scheme and a list of all employed parameterizations are provided as  
120 supplementary material.

121 In this study, the model is used to simulate an atmospheric updraft situation by following a  
122 preselected trajectory in temperature, relative humidity and pressure. It tracks the chemical  
123 composition of an amorphous aerosol particle as a function of time and depth below the  
124 particle surface in discretized layers, providing concentration profiles of water and organics at  
125 any given time. The equilibrium composition is calculated through a water activity  
126 parameterization that translates ambient relative humidity into equilibrium mass fractions of  
127 the bulk constituents. Mass fluxes from the far-surface into the near-surface gas phase, onto  
128 the particle surface, into as well as between bulk layers are coupled in flux-based differential  
129 equations, which are solved with an ordinary differential equation solver using Matlab  
130 software (ode23tb).

## 131 2.1.1 Ice nucleation modules

132 Besides water diffusion, the model is able to simulate ice nucleation and growth. However,  
133 the initial numerical solution of the differential equations treats merely water uptake into the  
134 particle. The model registers an ice nucleation event when all necessary conditions in ambient  
135 relative humidity and water activity are satisfied. From this point onwards, the model  
136 simulates ice crystal growth by deposition of water molecules from the gas phase.

137 For homogeneous ice nucleation, a stochastic approach based on classical nucleation theory  
138 has been chosen. An ice nucleation event is triggered when the probability of the particle  
139 being liquid ( $P_{\text{liq}}$ ) falls below 50 %.  $P_{\text{liq}}$  is the product of the individual probabilities in all  $n$   
140 layers, using the homogeneous nucleation rate coefficient for each layer  $J_{\text{hom},n}$  as  
141 parameterized by Koop et al. (2000). The nucleation rate then translates into  $P_{\text{liq}}$  by  
142 multiplication with layer volume  $V_n$  and (numerical) integration time step  $dt$ :

$$P_{\text{liq,tot}}(t) = \int_{t_0}^t \prod_{n=1}^L (1 - J_{\text{hom},n}(t) \cdot V_n(t)) dt \quad (1)$$

143 Heterogeneous nucleation is assumed to occur once a certain freezing threshold is exceeded.  
144 In this work, we distinguish between heterogeneous ice nucleation thresholds for sucrose and  
145 SOA, which have been shown to occur at different ice supersaturations, as summarized by  
146 Schill et al. (2014). For sucrose, we apply a linear fit to nucleation data from Baustian et al.  
147 (2013), whereas for SOA we fit the nucleation data of naphthalene SOA from Wang et al.  
148 (2012) and those of aqSOA from Schill et al. (2014). The fit results are shown in Fig. A1 in  
149 Appendix A.

150 To distinguish between deposition and immersion freezing, additional criteria are employed.  
151 For deposition nucleation, the necessary condition is solidness of the outermost layer of the  
152 particle, requiring the water activity to be below the quasi-equilibrium glass transition point.  
153 In case of immersion mode nucleation, a 1 nm thick region in the near-surface bulk is  
154 required to be entirely liquefied before nucleation can occur in the immersion mode. For this  
155 purpose, a 2 nm thick region below the particle surface is finely resolved by multiple bulk  
156 layers (cf. Fig. S1).

## 157 2.1.2 Bulk diffusion and bulk layer mixing

158 Bulk diffusion of water is treated as kinetic flux  $J_{bk,bk\pm 1}$  from one bulk layer ( $bk$ ) to the next  
159 ( $bk\pm 1$ ). Because layer thickness is not allowed to fall below molecular resolution,  
160 concentrations in adjacent layers can differ significantly. As in Zobrist et al. (2011), this  
161 heterogeneity is accounted for with a virtual mixing scheme for the determination of bulk  
162 diffusivities between layers. In this scheme, the composition of a mixture of two subsequent  
163 bulk layers is determined and the bulk diffusion coefficient calculated according to the  
164 effective composition along the diffusion path. Scenarios with very low diffusivities and  
165 hence steep concentration gradients thus lead to situations in which a liquefied layer (high  
166 bulk diffusivity of water,  $D_{H_2O}$ ) “softens” the subsequent glassy layer (low  $D_{H_2O}$ ), facilitating  
167 further diffusion. Such a process can be seen analogously to a dissolution process, in which  
168 the glassy matrix dissolves into nearby water-rich regions.

169 Diffusion of the organic matrix has been neglected for this study, because the organic  
170 molecules investigated here can be expected to diffuse much slower than water molecules.  
171 Also, in the glassy state, the organic molecules diffuse on a much longer timescale compared  
172 to the experimental time scale of minutes to hours [cf. Shiraiwa et al. (2011), Koop et al.  
173 (2011)].

## 174 2.1.3 Surface monolayers and surface softening

175 The original KM-GAP uses a double monolayer approach to describe the particle surface,  
176 comprising a sorption layer and a quasi-static surface layer. In this study the quasi-static  
177 surface layer was replaced by a near-surface volume layer similar to that used in Shiraiwa et  
178 al. (2013a), which is more suitable for systems with low diffusivity.

179 Surface-adsorbed water can lead to softening of the solid surface (Koop et al., 2011), thereby  
180 facilitating exchange between surface and first near-surface bulk layer. In the model, this is  
181 accounted for by introducing a surface softening scheme that estimates the surface-to-bulk  
182 transport rate by mixing a hypothetical water monolayer with a hypothetical bulk monolayer  
183 containing water and bulk material. Using the momentary molar fractions of water ( $x_{b1,H_2O}$ )  
184 and organics ( $x_{b1,org}$ ) of the near-surface bulk layer, the effective surface coverages of water  
185 ( $\theta_{ss,H_2O}$ ) and organics ( $\theta_{ss,org}$ ) at the surface bulk layer can be described as:

$$\theta_{ss,i} = \frac{x_{b1,i} \cdot \sigma_i}{x_{b1,org} \cdot \sigma_{org} + x_{b1,H2O} \cdot \sigma_{H2O}} \quad (2)$$

186 where  $\sigma_i$  is the molecular cross section of species  $i$  [i.e. water (H<sub>2</sub>O) or organics (org)],  
 187 respectively. The weight fraction of organics in the “softened” surface is then given by:

$$w_{ss,org,mix} = \frac{\frac{\theta_{ss,org}}{\sigma_{org}} \cdot M_{org}}{\frac{\theta_{ss,org}}{\sigma_{org}} \cdot M_{org} + \left(\frac{\theta_{ss,H2O} + 1}{\sigma_{H2O}}\right) \cdot M_{H2O}} \quad (3)$$

188 where  $M_{org}$  and  $M_{H2O}$  are the molar mass of organics and water. This process facilitates the  
 189 initial water uptake into a glassy particle and leads (in most cases) to a sub-surface layer that  
 190 is in equilibrium with the surrounding gas phase. In the temperature range relevant for  
 191 immersion freezing, liquefaction of the surface was always obtained at the quasi-equilibrium  
 192 glass transition point due to the surface softening mechanism. At lower temperatures however  
 193 (deposition regime), the particle surface was not always in quasi-equilibrium with ambient  
 194 humidity.

195

## 196 **2.2 Estimation of water diffusivity in SOA**

197 For model systems other than sucrose/water, no direct parameterization of water diffusivity in  
 198 the full atmospherically relevant temperature and composition range is available to date. For  
 199 compounds chemically similar to sucrose (i.e. organic polyols and acids), we present a  
 200 scheme that enables estimation of bulk diffusivity data from glass transition and  
 201 hygroscopicity data. Bulk diffusivity of water is parameterized using a Vogel-Fulcher-  
 202 Tamman (VFT) approach (Vogel, 1921; Fulcher, 1925; Tamman and Hesse, 1926). The  
 203 estimation scheme utilizes the structure of the VFT equation, Eq. (S9), and the physical  
 204 interpretation of its parameters. The method can be described by the following set of  
 205 assumptions:

- 206 1. Two similar organic substances act similar in the way they approach the glass  
 207 transition and thus have a similar fragility:  $B_{org,1} \approx B_{org,2}$ .
- 208 2. The same two substances have a similar diffusion coefficient in the high temperature  
 209 limit:  $A_{org,1} \approx A_{org,2}$ .

210 3. A difference in glass transition temperatures between the two substances indicates a  
211 difference in Vogel temperatures of same direction and (relative) magnitude

$$\frac{T_{0,\text{org},1}}{T_{0,\text{org},2}} \approx \frac{T_{g,\text{org},1}}{T_{g,\text{org},2}} \quad (4)$$

212 Thus, diffusivities within an organic substance can be estimated by knowledge of its glass  
213 transition curve relative to a known standard with similar chemical functionality. This  
214 approach requires knowledge of three parameters for inferring water diffusivity over the full  
215 temperature and composition range: the hygroscopicity coefficient  $\kappa_{\text{org}}$ , the glass transition  
216 temperature of the pure organic  $T_{g,\text{org}}$  and the Gordon-Taylor coefficient  $k_{\text{GT}}$  of the aqueous  
217 organic mixture. For justification, more information on this procedure and a description of  
218 how the required input parameters are obtained, see Appendix A. For validation of the  
219 estimation scheme, we provide applications to literature ice nucleation experiments in  
220 Appendix B.

## 221 3 Results and discussion

### 222 3.1 Particle Morphology

223 We investigate ice nucleation in glassy organic aerosols induced by changing ambient  
224 conditions during the updraft of an air parcel. In updraft events, adiabatic cooling leads to a  
225 decrease in temperature and a corresponding increase of relative humidity (RH).  
226 Humidification of air leads to water uptake into the particle phase, causing a humidity-  
227 induced phase transition that for glassy aerosol particles has been termed *amorphous*  
228 *deliquescence* (Mikhailov et al., 2009). This process is often kinetically limited by diffusion  
229 of water in the particle phase (Zobrist et al., 2011), so that a particle can be out of equilibrium  
230 when the time scale of humidification is shorter than that of diffusion.

231 Amorphous deliquescence is a self-accelerating process since water acts as a plasticizer in the  
232 organic matrix (Mikhailov et al., 2009; Zobrist et al., 2011): Water molecules taken up by the  
233 particle reduce the particle's viscosity and, hence, increase bulk diffusivity locally, thus  
234 accelerating the uptake of further molecules. The microphysical consequences of this  
235 mechanism are illustrated in Fig. 1, which shows the temporal evolution of particle  
236 morphology of a glassy organic aerosol particle exposed to a gradual increase in relative  
237 humidity (simulated atmospheric updraft, see also Movie S1). **The quasi-equilibrium glass**  
238 **transition of the aqueous organic,  $RH_g$ , is shown in grey.** With “quasi-equilibrium glass  
239 transition“, we denote the conditions under which a binary organic-water system would  
240 undergo amorphous deliquescence when humidification occurs sufficiently slow so that  
241 equilibrium between ambient RH and water activity is always maintained. Humidification  
242 may be fast enough to cause a difference in phase state from equilibrium: Water activity,  
243 colour-coded **from** dark blue (low water activity) to light blue (high water activity), trails  
244 behind ambient RH due to kinetic limitations in water diffusivity (Koop et al., 2011). Note  
245 that when using a constant  $D_{H_2O}$ , diffusion gradients appear less pronounced (cf. Fig. S2 and  
246 Movie S2). Hence, self-accelerating water diffusion leads to a sharpening of the diffusion  
247 gradient that can be close to the molecular length scale (Zobrist et al., 2011).

248 Several morphological stages can be distinguished during the humidification process **in Fig. 1**.  
249 Starting from a homogeneous, glassy particle **(1)**, an increase in RH first leads to liquefaction  
250 of a thin outer layer and emergence of a core-shell morphology **(2)**. This liquid outer layer  
251 grows in equilibrium with ambient relative humidity and also extends towards the particle

252 centre by diffusion of water into the glassy organic matrix (3), leading to shrinkage of the  
253 residual glassy core until the particle is fully deliquesced (4). Thus, during the continuous  
254 amorphous deliquescence process two characteristic instants can be distinguished, each  
255 occurring at a different humidity: We define the *Partial Deliquescence Relative Humidity*  
256 (PDRH) as the point where a thin aqueous outer shell of the particle is homogeneously mixed  
257 and the shell's water activity is larger than that of the quasi-equilibrium glass transition. In  
258 this study we set the thickness of this surface shell to 1 nm, corresponding to about 5  
259 monolayers of water. We define the *Full Deliquescence Relative Humidity* (FDRH) as the  
260 point where its water activity corresponds to that of a liquid (i.e. it is larger than that of the  
261 quasi-equilibrium glass transition) and the water activity gradient from the surface to the  
262 particle core is less than 5 %. Note that in the case of a sufficiently slow updraft, both PDRH  
263 and FDRH would occur at  $RH_g$ . In fact, the KM-GAP simulations suggest that, with updraft  
264 velocities typical for atmospheric conditions (e.g.  $0.01 - 10 \text{ m s}^{-1}$ ), PDRH often coincides  
265 with  $RH_g$ . In contrast, FDRH often extends far into the liquid region of the phase diagram,  
266 indicating the importance of kinetic limitations and implying that particles can contain glassy  
267 cores even at relative humidities above  $RH_g$  due to slow water diffusion.

### 268 3.2 Ice nucleation regimes

269 Next, we investigate by kinetic model simulations the competition between amorphous  
270 deliquescence and ice nucleation during an atmospheric updraft. For our initial calculations  
271 we use sucrose as a proxy for organic aerosols since detailed physico-chemical  
272 parameterizations for water diffusivity, the RH-dependent equilibrium composition as well as  
273 glass transition data are available (Zobrist et al., 2011). The heterogeneous ice nucleation  
274 onset ( $RH_{het}$ ) for sucrose was obtained from ice nucleation experiments by Baustian et al.  
275 (2013) and is shown as brown dashed lines in Fig. 2. Here we use the ice saturation ratio  $S_{ice}$   
276 as an indicator of humidity because it scales with RH according to  $S_{ice} = p_{liq,0}(T) / p_{ice}(T) \cdot RH$ ,  
277 but is also a more direct indicator of the supersaturation of ice.

278 Figure 2A shows results obtained with KM-GAP simulating the updraft of 100 nm sucrose  
279 particles for a wide range of temperatures. Each simulated trajectory started at ice saturation  
280 ( $S_{ice} = 1$ ), as is often the case for cloud chamber or environmental cell experiments (Murray et  
281 al., 2010; Wang et al., 2012). Temperature was decreased so that the resulting humidification

282 rate was constant at  $1 \text{ \% RH min}^{-1}$ , corresponding to an atmospheric updraft of about  $0.2 \text{ m s}^{-1}$ ,  
283  $^1$ , typical of atmospheric gravity waves (Jensen et al., 2005).

284 As expected FDRH of sucrose particles, indicated by the red solid line, occurs significantly  
285 above  $\text{RH}_g$  at all temperatures. The intersection of  $\text{RH}_{\text{het}}$  with  $\text{RH}_g$  defines the upper  
286 temperature limit for deposition nucleation. Below this temperature, a sucrose particle is a  
287 glassy solid when  $\text{RH}_{\text{het}}$  is reached, and hence deposition ice nucleation may occur. Above  
288 this temperature, the particle is partially deliquesced when approaching  $\text{RH}_{\text{het}}$  and the glassy  
289 core of the particle may act as an IN for immersion freezing. The upper limit of the immersion  
290 freezing regime is given by the intersection of  $\text{RH}_{\text{het}}$  with the FDRH line. Above this  
291 temperature, particles are already fully deliquesced once  $\text{RH}_{\text{het}}$  is reached. Hence, these  
292 particles do not nucleate ice heterogeneously and freeze only at the homogeneous ice  
293 nucleation limit (green dashed line; Koop et al., 2000). Finally at  $\sim 232 \text{ K}$ , the homogeneous  
294 ice nucleation limit coincides with water saturation (solid black line) and above this  
295 temperature the aerosol particles activate into cloud droplets consisting of supercooled water,  
296 thus representing the upper limit of the homogeneous ice nucleation regime.

297 The delay between the nominal quasi-equilibrium glass transition  $\text{RH}_g$  and the actual full  
298 deliquescence at FDRH is governed by the competition between humidification rate  
299 (synonymous to updraft velocity) and timescale for water diffusion within the particle bulk.  
300 FDRH will shift towards higher relative humidities when higher humidification rates are  
301 employed, as shown in Fig. 2B. For example, increasing the rate of humidification to  $10 \text{ \%}$   
302  $\text{RH min}^{-1}$ , a value corresponding to an updraft velocity of about  $2 \text{ m s}^{-1}$  and commonly  
303 reached in convective updrafts (Jensen et al., 2005), shifts the FDRH line upwards (solid dark  
304 blue line) and thus its intersection with the  $\text{RH}_{\text{het}}$  line towards higher temperatures.  
305 Accordingly, decreasing the updraft velocity to  $0.02 \text{ m s}^{-1}$ , a value found in large-scale,  
306 synoptic updrafts (Jensen et al., 2005), leads to FDRH (solid light blue line) much closer to  
307 the quasi-equilibrium glass transition  $\text{RH}_g$ . Moreover, an increase in particle size delays the  
308 deliquescence process (indicated by the solid purple line), since it increases the timescale of  
309 diffusion. The range of the immersion freezing regime thus strongly depends on ambient  
310 conditions and is extended towards higher temperatures in fast updrafts and for large particles.  
311 Laboratory ice nucleation measurements with sucrose particles (Baustian et al., 2013) are  
312 used to validate our model calculations of ice nucleation regimes in Fig. 2C. Baustian et al.  
313 used optical microscopy in conjunction with a cold stage to detect ice nucleation on glassy

314 sucrose particles (4  $\mu\text{m}$  diameter) during humidification (1 % RH  $\text{min}^{-1}$ ), leading to the  
315 nucleation onsets shown in Fig. 2C (brown markers). A range of simulations mimicking the  
316 experimental conditions at different starting temperatures leads to a continuous FDRH curve  
317 (solid blue line) over the entire temperature range. For details on the calculations see  
318 Appendix B. The modelled FDRH curve correctly confines the region below which  
319 heterogeneous ice nucleation is observed in the experiments. Based on our calculations, the  
320 experimental data points below  $\text{RH}_g$  (full brown circles) can be assigned to the deposition  
321 nucleation regime, whereas points between  $\text{RH}_g$  and FDRH (open brown circles) can be  
322 assigned to immersion freezing. Additional analyses for validation have been performed for  
323 other types of organic particles (Figs. B1 and B2).

### 324 3.3 Biogenic and anthropogenic SOA

325 In order to apply our kinetic model to ice nucleation in secondary organic aerosol (SOA),  
326 estimates of  $D_{\text{H}_2\text{O}}$  in SOA material have been inferred. Four major SOA precursors were  
327 chosen to represent biogenic and anthropogenic origin, respectively:  $\alpha$ -pinene and isoprene,  
328 as well as naphthalene and dodecane. Each of these SOA is represented by a choice of marker  
329 compounds taken from the literature (cf. Table S1). Water diffusivities are estimated utilizing  
330 the scheme described in Sect. 2.2. The heterogeneous ice nucleation onset ( $\text{RH}_{\text{het}}$ , brown  
331 dashed line) for SOA was obtained from laboratory measurements by Wang et al. (2012) and  
332 Schill et al. (2014) as derived in Fig. A1. Hygroscopicities of the various SOA were taken  
333 from Lambe et al. (2011), who suggested that  $\kappa_{\text{org}}$  can be parameterized independently of SOA  
334 type as function of O/C ratio. In all simulations, particles of 100 nm diameter were humidified  
335 at a rate of 1 % RH  $\text{min}^{-1}$ .

336 Figure 3A shows the simulation results of FDRH for all four precursor types. Naphthalene  
337 SOA is observed to be fully deliquesced latest due to the high estimated glass transition  
338 temperature and low hygroscopicity (cf. Table A1), followed by  $\alpha$ -pinene and isoprene.  
339 Dodecane SOA showed the earliest deliquescence, reflecting the low glass transition  
340 temperature of pure dodecane SOA of  $\sim 210$  K. By comparison of FDRH with measured  $\text{RH}_{\text{het}}$   
341 on SOA, compound-specific upper temperature limits for heterogeneous ice nucleation on  
342 SOA particles can be determined (arrows on x-axis, values are given in Table S2).  
343 Uncertainty estimates for FDRH and  $\text{RH}_g$  of all four precursors classes are given in Fig. S4.

344 For the calculations in Fig. 3A, we chose an average oxidation state typically observed for  
345 SOA from the respective precursor. The atomic oxygen to carbon ratio (O/C) increases upon  
346 chemical ageing, thereby affecting hygroscopicity (Lambe et al., 2011) and glass transition  
347 temperature (Fig. A2). The resulting effects of chemical ageing on modelled FDRH are  
348 shown exemplarily for  $\alpha$ -pinene and dodecane SOA in Fig. 3B and C, respectively. For  $\alpha$ -  
349 pinene SOA (B), a higher O/C results in hardening of the organic material with ageing,  
350 leading to a FDRH increase, whereas for dodecane SOA (C) a higher O/C results in softening,  
351 thus leading to earlier deliquescence and a FDRH decrease.

352 The observed effects can be explained by the competition between a simultaneous increase of  
353 hygroscopicity with O/C and an increasing glass transition temperature of the pure organic  
354 matrix due to stronger molecular interactions in the highly oxidized organic material. A  
355 higher glass transition value enhances the rigidity of the pure organic matrix, whereas a  
356 higher hygroscopicity enhances the amount of water taken up by the aqueous organic mixture  
357 at a given humidity and thus its plasticizing effect.

358 Figure 4 illustrates this competition by displaying estimated characteristic timescales of water  
359 diffusion in 100 nm diameter SOA particles at 220 K as a function of hygroscopicity ( $\kappa_{\text{org}}$ )  
360 and glass transition temperature of the pure organic matrix ( $T_{\text{g,org}}$ ). Dotted contour lines show  
361 characteristic mass transport times associated with the diffusion coefficient  $D_{\text{H}_2\text{O}}$  (Shiraiwa et  
362 al., 2011). Coloured oval shapes indicate estimated ranges of  $\kappa_{\text{org}}$  and  $T_{\text{g,org}}$  for the four SOA  
363 precursor classes, for three different oxidation states each (cf. Table A1). The arrows pointing  
364 from the lowest to the highest oxidation state reveal that both  $\kappa_{\text{org}}$  and  $T_{\text{g,org}}$  increase with O/C.  
365 The slope of these arrows when compared to the slope of the contour lines indicates whether a  
366 compound undergoes hardening (steeper slope) or softening (**shallower slope**) during the  
367 ageing process. Apparently, both biogenic SOA types undergo hardening upon ageing,  
368 whereas the two anthropogenic SOA types undergo softening, with the strongest effects for  
369 pinene and dodecane SOA.

370 The area between 1 s and 1 h represents the time scale of atmospheric updraft processes. For  
371 SOA in this range, diffusion processes occur on the same time scales as typical air parcel  
372 updrafts and the predominant cloud formation process depends strongly on atmospheric  
373 conditions. All four SOA types fall within or beneath this range, indicating the importance of  
374 the actual updraft velocity for ice nucleation on glassy aerosols. But it is also obvious that

375 SOA particles from naphthalene are most likely to be subject to kinetic effects and may thus  
376 act as IN.

### 377 **3.4 Model uncertainties**

378 The model results presented in this study are subject to various types of uncertainty. Among  
379 these are uncertainties arising from model assumptions such as the validity of first-order  
380 Fickian diffusion and the applied schemes for bulk mixing and surface softening (Sects. 2.1.2  
381 and 2.1.3). At present there is a lack of fundamental chemical and physical knowledge for  
382 describing these processes in aqueous binary or multicomponent systems. We note, however,  
383 that the approach taken here is in agreement with the sparse data on water diffusivities in  
384 aqueous organic systems (Zobrist et al., 2011; Shiraiwa et al., 2013b; Lienhard et al., 2014;  
385 Price et al., 2014). Model results obtained for aqueous sucrose (Fig. 2) are expected to be  
386 reliable because the thermodynamic and kinetic parameters of this benchmark system are well  
387 studied and agree within the literature (e.g. Zobrist et al., 2011; Price et al., 2014); on the  
388 other hand, model results obtained for SOA (Fig. 3) are subject to larger uncertainties as  
389 detailed in the following.

390 The model neglects liquid-liquid phase separation in the aqueous organic phase (You et al.,  
391 2014) by assuming that all SOA components are miscible with water over the entire  
392 concentration and temperature range. We note that for SOA types that typically show only  
393 low O/C ratios (e.g. SOA from long chain aliphatic precursors such as dodecane), insoluble  
394 fractions may become important for ice nucleation (see discussion in Sect. B2).

395 Volatilization of organic material has not been included in the calculations presented above  
396 since vapour pressures of typical SOA marker compounds are low under the low temperature  
397 conditions employed in this study (Huisman et al., 2013; O'Meara et al., 2014).

398 Self-diffusion of SOA material has been neglected as diffusion time scales of large organic  
399 molecules exceed those of small guest molecules in the SOA matrix by orders of magnitudes  
400 (Koop et al., 2011; Shiraiwa et al., 2011).

401 Minor model uncertainty comes from parameters determining the volume concentration of  
402 organic molecules at a given organic mass fraction, i.e. average molar mass  $M_{\text{org}}$  of the  
403 organics and density of the aqueous organic mixture (cf. Table S3). Variation by  $100 \text{ g mol}^{-1}$   
404 in  $M_{\text{org}}$  showed no effect on model results, varying  $\rho_{\text{org}}$  by  $0.1 \text{ g cm}^{-3}$  showed only a slight  
405 influence on aerosol deliquescence humidity on the order of 1 % RH.

406 The arguably largest source of uncertainty is insufficient knowledge of the thermodynamic  
407 input parameters required for the diffusivity estimation scheme ( $\kappa_{\text{org}}$ ,  $T_{\text{g,org}}$ ,  $k_{\text{GT}}$ , cf. Appendix  
408 A). In addition to the general assumptions made in that scheme and the uncertainties in the  
409 sucrose parameterization used within the diffusivity estimation scheme, uncertainties in input  
410 parameters propagate into an uncertainty in  $D_{\text{H}_2\text{O}}$ , which we assess in Figs. S4 and S6. Figure  
411 S4 shows the uncertainty for each specific SOA precursor and a particular O/C ratio by  
412 propagating the maximum deviation estimates in  $\kappa_{\text{org}}$  and  $T_{\text{g,org}}$  given in Table A1. Figure S6  
413 shows the full uncertainty towards single model input parameters irrespective of precursor or  
414 oxidation state. Among these,  $\kappa_{\text{org}}$  seems to be the largest source of uncertainty as the model  
415 results are sensitive towards  $\kappa_{\text{org}}$  and its numerical value subject to a rather large variability  
416 for atmospherically relevant organic substances (Koop et al., 2011; Lambe et al., 2011;  
417 Rickards et al., 2013). Due to lack of consistent experimental data, a constant  $\kappa_{\text{org}}$  is used in  
418 this study to parameterize hygroscopicity over the entire concentration and temperature range.  
419 Thus, laboratory experiments that directly probe diffusivity within SOA at room temperature  
420 and also at low temperature are highly desirable, as it has been done for sucrose and few other  
421 single-compound proxies (Tong et al., 2011; Zobrist et al., 2011; Bones et al., 2012; Lienhard  
422 et al., 2014; Price et al., 2014). Moreover, experiment-based water activity parameterizations  
423 over a large temperature range are needed, because at least some water-soluble organic  
424 oligomers/polymers show a strong temperature dependence of water activity for aqueous  
425 mixtures of constant composition (Zobrist et al., 2003). Both such improvements would  
426 reduce the model uncertainty in future modelling studies substantially.

427 Another type of uncertainty arises from uncertainty in heterogeneous ice nucleation onsets.  
428 To date, little is known about the exact microphysical mechanism by which amorphous  
429 organics nucleate ice heterogeneously (Wagner et al., 2012; Marcolli, 2014; Schill et al.,  
430 2014). Reported ice nucleation onsets of glassy particles span wide ranges and are most likely  
431 substance or substance class-specific (Wilson et al., 2012; Schill et al., 2014). Thus, further  
432 laboratory experiments are needed that reveal details on the ice nucleation mechanism and  
433 that allow predictions of ice nucleation ability for a wide variety of substances.

434

#### 435 **4 Atmospheric implications of glassy organic IN**

436 Organic aerosols can induce cloud formation via many different pathways depending on  
437 ambient conditions and composition. At high temperature and high humidity, liquid organic  
438 particles can act as cloud condensation nuclei (CCN). At lower temperatures, they facilitate  
439 formation of ice crystals. Figure 5 summarizes how the phase state and morphology of  
440 atmospheric organic aerosol particles may vary upon changes in ambient relative humidity  
441 (humidity-induced phase transitions). Upon humidifying, the phase state changes from  
442 amorphous solid (glassy) over a partially-deliquesced state with a solid core residual coated  
443 by a liquid shell to a fully-deliquesced liquid. Upon drying the transition may occur via an  
444 inverse core-shell morphology, i.e. a liquid coated by a solid shell. Consequently, the particle  
445 phase state determines the active ice nucleation pathway: Glassy solids can nucleate ice in the  
446 deposition mode, partially deliquesced particles with core-shell morphologies may act as IN  
447 in the immersion mode and liquid particles nucleate ice homogeneously, at significantly  
448 higher ice supersaturation.

449 From the SOA types investigated in this study, aromatic SOA or highly aged  $\alpha$ -pinene SOA  
450 may persist in a glassy state to the highest temperatures and humidities and may thus facilitate  
451 heterogeneous ice nucleation at temperatures of up to 225 K. Below 210 K, SOA from all  
452 precursors are expected to be in the glassy state required for heterogeneous ice nucleation.  
453 Our microphysical simulations suggest a potential anthropogenic influence of IN from  
454 emission of aromatic VOCs and by providing high oxidative capacities in urban areas leading  
455 to an increase of ice nucleation in and on glassy organic particles.

456 Compared to typical atmospheric IN such as dust, soot and biological particles, glassy organic  
457 particles require temperatures below  $\sim 230$  K to nucleate ice heterogeneously (Hoose and  
458 Möhler, 2012). This restriction confines their atmospheric activity range to the upper  
459 troposphere – lower stratosphere region since the glassy state is prevalent only up to  
460 temperatures of about 200 – 240 K under typical atmospheric humidities ( $S_{\text{ice}} \approx 1$ ), depending  
461 on composition.

462 In this study we show a strong interplay between diffusion time scales in the atmosphere and  
463 atmospheric updraft speeds: the stronger the updraft and the larger the particle size, the more  
464 kinetic limitations delay the liquefaction of glassy particles. These findings also imply that an  
465 ice nucleation onset determined in laboratory studies needs to be interpreted carefully in order  
466 to apply it to realistic atmospheric parameters, i.e. humidification rate, particle size and

467 starting humidity. Kinetic limitations are already pronounced at the smallest atmospherically  
468 relevant updraft velocities of  $0.02 \text{ m s}^{-1}$ . When humidification is fast (e.g. in convective  
469 updrafts), the glassy state may persist well above its quasi-equilibrium boundaries. Our  
470 simulations on sucrose and SOA particles suggest a shift of humidity-induced glass transition  
471 to higher temperatures by about 5 K when updraft velocities are increased by a factor of 10.  
472 Also, the history of an organic particle has effects on its water uptake properties: Particles that  
473 were equilibrated at lower humidity are expected to deliquesce at higher ice supersaturation.  
474 In situations where particles are both, equilibrated in dry air ( $S_{\text{ice}} < 0.9$ ) and elevated quickly,  
475 upper temperature limits for immersion freezing on glassy organics might reach much higher  
476 values than the conservative estimates given in this study. Thus, also ice nucleation in mid-  
477 altitude clouds may be affected by this heterogeneous ice nucleation pathway.

478 This study outlines the basic physico-chemical relations and makes a first attempt in  
479 quantifying temperature limits for heterogeneous ice nucleation by four generic types of SOA,  
480 but further laboratory and modelling studies are needed to provide a comprehensive set of  
481 parameterizations to be used in atmospheric models. To assess the global importance of ice  
482 nucleation by SOA particles and to quantify the associated aerosol effects on climate, studies  
483 with large scale computational models are needed. As small scale kinetic processes cannot be  
484 treated explicitly in these kinds of models, parameterizations are required that include  
485 dependencies upon temperature, relative humidity, updraft velocity, particle size and  
486 composition.

487 **Appendix A: Details on the estimation of bulk diffusivities from glass transition**  
488 **and hygroscopicity data**

489 **A.1. Justification of the method**

490 Even though the estimation scheme described in Sect. 2.2 represents a rather crude estimation  
491 of water diffusivities, it builds on basic physical principals: In solutions of chemically similar  
492 organic substances (like the mixture of highly functionalized organic species in SOA), the  
493 types of molecular interactions are mostly hydrogen bonds and dispersion interactions,  
494 irrespective of the actual composition. Differences in diffusive properties are to a substantial  
495 degree due to factors such as molar mass and shape, both of which directly affect the glass  
496 transition temperature (Koop et al., 2011). The way by which the glass transition is  
497 approached is not affected strongly by the substance type, as all organic compounds relevant  
498 for SOA are *fragile* glass-formers (Angell, 1985). The proposed method is consistent with the  
499 following previous studies:

500 Rampp et al. (2000) used NMR spectroscopy to determine water diffusion coefficients in  
501 different carbohydrate matrices (sucrose, allosucrose, leucrose, trehalose) and fitted VFT  
502 parameters to the temperature and concentration-dependent data sets. Overall, similar VFT  
503 parameters  $A$  and  $B$  were found for these chemically similar substances, even though  $D_{\text{H}_2\text{O}}$   
504 seemed to depend strongly on organic mass fraction, thus supporting assumptions 1 and 2  
505 above. The observed concentration dependence was described almost exclusively by a change  
506 in  $T_0$ , with only small trends in  $A$  and minor variation in  $B$ , possibly due to experimental error,  
507 thus supporting assumption 3.

508 Angell (1997) investigated the correlation of Kauzmann temperatures  $T_k$  with Vogel  
509 temperatures  $T_0$  and found their ratio to be close to unity. The ratio of  $T_g$  to  $T_0$  has been shown  
510 to be confined to a narrow range between  $1.07 < T_g/T_0 < 1.82$  for a wide variety of strongly  
511 different substances. This ratio seems to be correlated in magnitude to the substances fragility  
512 (i.e. VFT parameter  $B$ ), with high fragilities implying high  $T_g/T_0$  ratios. Reversely the  
513 assumption of similar fragilities (assumption 2) directly points towards similar  $T_g/T_0$  ratios  
514 (assumption 3). Accordingly, deducing Vogel temperatures  $T_0$  from glass transition properties  
515 seems reasonable.

## 516 **A.2. Estimation of glass transition temperatures $T_{g,org}$**

517 The proposed estimation scheme enables the prediction of bulk diffusion coefficients only  
518 from knowledge of glass transition values for the desired RH range. The glass transition curve  
519 can be described by three parameters: the glass transition temperature of the pure molecular  
520 compound  $T_{g,org}$ ; the Gordon-Taylor constant  $k_{GT}$  of the aqueous organic mixture; and the  
521 hygroscopicity  $\kappa_{org}$  for translating composition into water activity.  $T_{g,org}$  exhibits a linear  
522 correlation with melting point  $T_m$ , also known as the Boyer-Beaman rule (Koop et al., 2011).  
523  $T_m$  can be estimated by group contribution models with knowledge of its chemical structure.  
524 We use the melting point prediction model of UPPER (Unified Physical Property Estimating  
525 Relationships) as presented by Jain et al. (Jain and Yalkowsky, 2006; Jain et al., 2004).

526 Table S1 shows our choice of marker substances for four different types of SOA along with  
527 molar mass, melting points predicted with UPPER and predicted glass transition values based  
528 on the Boyer-Beaman rule. The SOA groups were chosen to include SOA from the most  
529 commonly studied precursors and are derived from one specified precursor substance each.  
530 The groups “ $\alpha$ -Pinene” and “Isoprene” represent SOA from biogenic origin, whereas  
531 “Naphthalene” and “Dodecane” are our choice for precursors of anthropogenic origin.

532 The group “ $\alpha$ -Pinene” contains compounds characteristic for photooxidation and ozonolysis  
533 of the biogenic SOA precursor  $\alpha$ -pinene, which has been chosen as proxy for the different  
534 monoterpene VOCs responsible for biogenic SOA formation. The list contains compounds  
535 with the highest yields according to MCM-based simulations of Shilling et al. (2009) as well  
536 as of Zuend and Seinfeld (2012), who also included two dimer substances. Furthermore, we  
537 included 3-MBTCA, a highly oxidized pinene derivative found in ambient samples  
538 (Szmigielski et al., 2007) as well as terpenylic acid, a tracer for rather fresh SOA, along with  
539 two of its derivatives (Claeys et al., 2009).

540 The group “Isoprene” contains isoprene-derived compounds found in ambient and laboratory  
541 aerosol as suggested by Surratt et al. (2006) and references therein. These authors also  
542 proposed a high contribution of esterification products with 2-methylglyceric acid as  
543 monomeric unit to SOA mass. Table S1 lists these oligomers up to the tetramer level, where  
544 predicted glass transition values start to level off.

545 The group “Naphthalene” represents typical products originating from the oxidation of  
546 anthropogenic aromatic precursors. Note that for highly functionalized aromatic compounds,

547 UPPER predicts unusually high values for  $T_m$ , which are inconsistent with observations. For  
548 example, phthalic acid melts under decomposition (presumably anhydrate formation) at 403 K  
549 (Lide, 2005), whereas UPPER suggests a melting point of about 539 K. For this reason, we  
550 used only those naphthalene oxidation products for which literature melting points are known,  
551 such as the substances given in Saukko et al. (2012) and a number of compounds listed in  
552 Kautzman et al. (2010). Note that for the same reason we did not include oligomerization  
553 products to the “Naphthalene” group. Oligomerization is however also expected for aromatic  
554 SOA, shown e.g. by Kalberer et al. (2004), which would lead to higher  $T_{g,org}$  (Koop et al.,  
555 2011). For these reasons, our estimates for aromatic SOA materials may be regarded as a  
556 conservative estimate.

557 The group “Dodecane” in Table S1 lists oxidized organics derived from the C12 straight  
558 chain alkane to represent the family of similar compounds originating from aliphatic VOCs of  
559 anthropogenic origin. The list is a selection from the comprehensive chemical mechanism in  
560 Yee et al. (2012) and three compounds from those suggested by Zhang et al. (2014).

561 The resulting glass transition values are presented in Fig. A2 as a function of atomic O/C ratio  
562 and a clear positive correlation is observed within each group of compounds. **Such a**  
563 **correlation between  $T_{g,org}$  and O/C has been supported by recent  $T_g$  measurements of mixtures**  
564 **of  $\alpha$ -pinene derived oxidation compounds (Dette et al., 2014). In Fig. A2, the solid lines are**  
565 **obtained by linear regressions of the glass transition values** using a bisquare weighting  
566 function and shaded areas are confidence intervals at the  $1\sigma$  level. The chosen marker  
567 compounds occupy compound-specific ranges of O/C values, which is in part due to a  
568 different carbon number in the precursor molecule. To estimate a value characteristic for a  
569 mixture of the single compounds, we choose three values of O/C ratios that are typical for the  
570 respective group and take at each of those values the corresponding  $T_{g,org}$  that arises from the  
571 linear fit. The errors are then given by the extension of confidence bands at each point. The  
572 results are shown in Table A1.

573

### 574 **A.3. Estimation of Gordon-Taylor constants $k_{GT}$**

575 Gordon-Taylor constants are necessary to estimate the glass transition temperatures of  
576 compound mixtures. Zobrist et al. (2008) determined Gordon-Taylor constants for a variety of  
577 atmospherically relevant substances and SOA proxies. However, data are sparse when  
578 compared to the wide structural variety of compounds in SOA and no clear correlation can be

579 drawn from the molecular structure. For this reason, Koop et al. (2011) recommended the  
580 usage of a mean Gordon-Taylor constant of  $k_{GT} = 2.5 \pm 1$  (cf. Table A1). Figure S6 shows the  
581 temperature dependence of FDRH in calculations similar to Figs. 2 and 3, this time using the  
582 best guess parameters recommended in Koop et al. (2011). The uncertainty in FDRH that  
583 arises from the given input parameter ranges is shown (grey shaded), but also the specific  
584 uncertainty from varying  $k_{GT}$  between 1.5 and 3.5 is highlighted (orange shaded).

585

#### 586 **A.4. Estimation of hygroscopicities $\kappa_{org}$**

587 The hygroscopicity of a compound can be expressed by a single parameter  $\kappa_{org}$ , which is  
588 strongly correlated to its degree of oxidation (Petters and Kreidenweis, 2007; Lambe et al.,  
589 2011). A typical value for  $\kappa_{org}$  in biogenic SOA particles collected in pristine rainforest  
590 environments is 0.1 (Gunthe et al., 2009), which was also used by Koop et al. (2011) for their  
591 estimation of glass transition values in biogenic SOA.

592 For estimation of  $\kappa_{org}$ , we use the parameterization of Lambe et al. (2011) that correlates the  
593 O/C ratio of secondary organic material to its hygroscopicity, Eq. (A1).

$$\kappa_{org} = (0.18 \pm 0.04) * O/C + 0.03 \quad (A1)$$

594 Each SOA precursor class is assigned a typical O/C value from previous investigations of  
595 marker compounds (cf. Fig A2) and results are shown in Table A1. With the knowledge of  
596  $T_{g,org}$ ,  $k_{GT}$  and  $\kappa_{org}$ , the entire glass transition curves for the four SOA types can be calculated,  
597 as visualized in Fig. S4. Dashed lines and grey shaded areas indicate ranges of uncertainty.

598

#### 599 **A.5. Evaluation of the method**

600 For evaluation of the performance of the diffusivity estimation scheme, we compare estimated  
601 diffusivity values with values obtained in experiments by Price et al. (2014). In these  
602 experiments, D<sub>2</sub>O-H<sub>2</sub>O exchange in an organic matrix at constant temperature and humidity is  
603 investigated by Raman spectroscopy. Figure S3 shows the experimentally determined  $D_{H_2O}$   
604 values for sucrose and levoglucosan in Price et al. (blue and purple markers) as well as the  
605  $D_{H_2O}$  parameterization from Zobrist et al. (2011) (blue solid line).  $D_{H_2O}$  in levoglucosan has  
606 also been estimated with the diffusivity estimation scheme (purple solid line), utilizing input

607 parameters from Zobrist et al. (2008) ( $T_{g,org} = 283.6$  K,  $k_{GT} = 5.2$ ). Water activity has been  
608 parameterized using the parameters in Table S4.

609 Experimental and estimated values coincide for the highest and lowest water activities but  
610 differ under medium conditions due to the different curvature of the base parameterization  
611 from Zobrist et al. that underlies all calculations. However, diffusivities differ only within at  
612 most two orders of magnitude, which is a considerably small deviation compared to the large  
613 set of approximations made here and the difference between experimental techniques.

## 614 **Appendix B: Application of the model to ice nucleation experiments in the** 615 **literature**

616

### 617 **B.1. Sucrose experiments**

618 Baustian et al. (2013) investigated sucrose particles deposited on a quartz substrate and  
619 humidified inside an experimental flow cell. After cooling and drying below the glass  
620 transition, particles with an average diameter of 4  $\mu\text{m}$  were humidified by cooling at a rate of  
621 0.1  $\text{K min}^{-1}$ . Humidification was initialized below ice saturation ( $S_{\text{ice}} < 0.9$ ). The resulting  
622 heterogeneous ice nucleation onsets (brown circles) are shown in Fig. 2C along with the full  
623 deliquescence relative humidity (FDRH, blue solid line) from multiple model runs (spacing: 2  
624 K) mimicking the experimental conditions. Simulations below 215 K (left black square  
625 marker) are found to nucleate in the deposition mode, whereas particles in runs between about  
626 215 K and 238 K (right black square marker) are assumed to undergo immersion freezing.  
627 This result is compliant with the experimental values, none of which exceeds a nucleation  
628 temperature of 235 K. Above 238 K full deliquescence occurs before the ice supersaturation  
629 required for heterogeneous ice nucleation (brown dashed line) is reached. Also, homogeneous  
630 ice nucleation is not possible anymore below the water saturation limit according to Koop et  
631 al. (2000; green dashed line), leaving no remaining ice nucleation pathway.

632

### 633 **B.2. Naphthalene SOA experiments**

634 Wang et al. (2012) generated SOA by oxidation of naphthalene by OH in a potential aerosol  
635 mass (PAM) reactor, deposited the particles on glass slides and investigated the onsets of  
636 water uptake and ice nucleation inside an ice nucleation cell that was mounted on a  
637 microscope. Experimental results are shown in Fig. B1 for three different SOA oxidation  
638 states: Low O/C (0.27) given in red, medium O/C (0.54) in green and high O/C (1.0) in blue.  
639 For the comparing model simulations, we employ our diffusivity estimation scheme with the  
640 glass transition parameterization for naphthalene given above. A humidification rate of 1 %  
641  $\text{RH min}^{-1}$  was employed and temperature varied accordingly to maintain a constant dew point.  
642 In Fig. B1, the lines of full deliquescence relative humidity (FDRH) divide the measured  
643 heterogeneous ice nucleation onsets into two groups, irrespective of the degree of oxidation  
644 used in the simulation. Heterogeneous nucleation at or below 225 K is consistent with

645 simulation results (closed diamonds), whereas ice nucleation at or above 230 K cannot be  
646 explained with the estimated water diffusion properties (open diamonds). According to the  
647 model simulation, naphthalene SOA should be already deliquesced at temperatures and RH  
648 where ice nucleation is still experimentally observed. The model simulations thus suggest that  
649 a different ice nucleation mechanism **that does not require organic material in a glassy state**  
650 **was active in these experiments. Possibly, insoluble products from Naphthalene OH oxidation**  
651 **remained solid in the otherwise fully deliquesced particle and nucleated ice heterogeneously**  
652 **with lower efficiency. Such a process is not considered in the model, which does not resolve**  
653 **single compounds and treats Naphthalene SOA as homogeneous mixture at all times.**

654 The reliability of the method is confirmed by comparing experimental and modelled water  
655 uptake onsets that show very good correlation. The modelled water uptake onset was defined  
656 as the point where the particle diameter had increased by 100 nm to take into account the fact  
657 that experimental onsets were determined by visible inspection under a light microscope.

658

### 659 **B.3. Citric acid experiments**

660 Murray et al. (2010) observed the process of heterogeneous ice nucleation on glassy aerosols  
661 by investigating citric acid particles in the AIDA cloud chamber. The experimentally  
662 determined onsets of heterogeneous (orange diamonds) and homogeneous ice nucleation  
663 (green circles) are shown in Fig. B2 along with results of simulations mimicking the  
664 experimental conditions. In the calculations, we assumed a particle diameter of 150 nm and a  
665 humidification rate of 12 % RH min<sup>-1</sup>, corresponding to a cooling rate of 1-2 K min<sup>-1</sup>.  
666 Humidification was initiated at  $S_{ice} = 1$  since the cloud chamber walls were covered with ice  
667 during the initial cooling process. We performed two series of simulations for two different  
668 water activity parameterizations available in the literature. According to the parameterization  
669 in Lienhard et al. (2012) (dashed lines), heterogeneous nucleation occurs exclusively above  
670 the (equilibrium) glass transition relative humidity  $RH_g$  and thus in the immersion freezing  
671 regime. With the parameterization from Koop et al. (2011) (solid lines), equilibrium glass  
672 transition and full deliquescence occur at later stages in the humidification process. According  
673 to this data, only the experimental data point at about 206 K would have occurred in the  
674 immersion mode.

675 At 212 K, ice nucleation occurs only homogeneously in Murray's experiments, indicated by  
676 the much later ice nucleation onset. The humidification run started with liquid aerosol

677 particles that showed retarded deliquescence, but were not able to nucleate ice  
678 heterogeneously.

679 **Author contributions**

680 T. B., M. S., U. P. and T. K. designed research; T. B., M. S. and T. K. developed the model;  
681 T. B. performed research; T. B. and T. K. analysed simulation data; T. B., M. S., U. P. and T.  
682 K. wrote the paper.

683

684 **Acknowledgements**

685 This work was funded by the Max Planck Society (MPG), the Deutsche  
686 Forschungsgemeinschaft through the Ice Nuclei Research Unit INUIT (FOR1525, Grant KO  
687 2944/2-1), and the European Commission under the PEGASOS project (grant no. 265148). T.  
688 B. was supported by the Max Planck Graduate Center with the Johannes Gutenberg-  
689 Universität Mainz (MPGC). The authors thank P. Spichtinger, U. K. Krieger, D. M. Lienhard,  
690 B. P. Luo, T. Peter, A. T. Lambe, S. S. Steimer, **D. A. Knopf** and H.-P. Dette for stimulating  
691 discussions.

692

693 **References**

694 Adler, G., Koop, T., Haspel, C., Taraniuk, I., Moise, T., Koren, I., Heiblum, R. H., and  
695 Rudich, Y.: Formation of highly porous aerosol particles by atmospheric freeze-drying in ice  
696 clouds, *Proc. Natl. Acad. Sci. USA*, 110, 20414-20419, 10.1073/pnas.1317209110, 2013.

697 Andreae, M. O., and Rosenfeld, D.: Aerosol-cloud-precipitation interactions. Part 1. The  
698 nature and sources of cloud-active aerosols, *Earth Sci. Rev.*, 89, 13-41,  
699 10.1016/j.earscirev.2008.03.001, 2008.

700 Angell, C. A.: in: *Relaxations in Complex Systems*, edited by: Ngai, K., and Wright, G. B.,  
701 National Technical Information Service, I.S. Department of Commerce, Springfield, VA,  
702 1985.

703 Angell, C. A.: Landscapes with megabasins: Polyamorphism in liquids and biopolymers and  
704 the role of nucleation in folding and folding diseases, *Physica D*, 107, 122-142,  
705 10.1016/s0167-2789(97)00077-8, 1997.

706 Baustian, K. J., Wise, M. E., Jensen, E. J., Schill, G. P., Freedman, M. A., and Tolbert, M. A.:  
707 State transformations and ice nucleation in amorphous (semi-)solid organic aerosol, *Atmos.*  
708 *Chem. Phys.*, 13, 5615-5628, 10.5194/acp-13-5615-2013, 2013.

709 Bones, D. L., Reid, J. P., Lienhard, D. M., and Krieger, U. K.: Comparing the mechanism of  
710 water condensation and evaporation in glassy aerosol, *Proc. Natl. Acad. Sci. USA*, 109,  
711 11613-11618, 10.1073/pnas.1200691109, 2012.

712 Claeys, M., Iinuma, Y., Szmigielski, R., Surratt, J. D., Blockhuys, F., Van Alsenoy, C., Boge,  
713 O., Sierau, B., Gomez-Gonzalez, Y., Vermeylen, R., Van der Veken, P., Shahgholi, M., Chan,  
714 A. W. H., Herrmann, H., Seinfeld, J. H., and Maenhaut, W.: Terpenylic Acid and Related

715 Compounds from the Oxidation of alpha-Pinene: Implications for New Particle Formation  
716 and Growth above Forests, *Environ. Sci. Technol.*, 43, 6976-6982, 10.1021/es9007596, 2009.

717 Cziczo, D. J., Froyd, K. D., Hoose, C., Jensen, E. J., Diao, M. H., Zondlo, M. A., Smith, J. B.,  
718 Twohy, C. H., and Murphy, D. M.: Clarifying the Dominant Sources and Mechanisms of  
719 Cirrus Cloud Formation, *Science*, 340, 1320-1324, 10.1126/science.1234145, 2013.

720 DeMott, P. J., Cziczo, D. J., Prenni, A. J., Murphy, D. M., Kreidenweis, S. M., Thomson, D.  
721 S., Borys, R., and Rogers, D. C.: Measurements of the concentration and composition of  
722 nuclei for cirrus formation, *Proc. Natl. Acad. Sci. USA*, 100, 14655-14660,  
723 10.1073/pnas.2532677100, 2003.

724 Dette, H. P., Qi, M. A., Schroder, D. C., Godt, A., and Koop, T.: Glass-Forming Properties of  
725 3-Methylbutane-1,2,3-tricarboxylic Acid and Its Mixtures with Water and Pinonic Acid, *J.*  
726 *Phys. Chem. A*, 118, 7024-7033, 10.1021/jp505910w, 2014.

727 Froyd, K. D., Murphy, D. M., Lawson, P., Baumgardner, D., and Herman, R. L.: Aerosols  
728 that form subvisible cirrus at the tropical tropopause, *Atmos. Chem. Phys.*, 10, 209-218, 2010.

729 Fulcher, G. S.: Analysis of recent measurements of the viscosity of glasses, *J. Am. Ceram.*  
730 *Soc.*, 8, 339-355, 10.1111/j.1151-2916.1925.tb16731.x, 1925.

731 Gunthe, S. S., King, S. M., Rose, D., Chen, Q., Roldin, P., Farmer, D. K., Jimenez, J. L.,  
732 Artaxo, P., Andreae, M. O., Martin, S. T., and Pöschl, U.: Cloud condensation nuclei in  
733 pristine tropical rainforest air of Amazonia: size-resolved measurements and modeling of  
734 atmospheric aerosol composition and CCN activity, *Atmos. Chem. Phys.*, 9, 7551-7575,  
735 10.5194/acp-9-7551-2009, 2009.

736 Hoose, C., and Möhler, O.: Heterogeneous ice nucleation on atmospheric aerosols: a review  
737 of results from laboratory experiments, *Atmos. Chem. Phys.*, 12, 9817-9854, 10.5194/acp-12-  
738 9817-2012, 2012.

739 Huisman, A. J., Krieger, U. K., Zuend, A., Marcolli, C., and Peter, T.: Vapor pressures of  
740 substituted polycarboxylic acids are much lower than previously reported, *Atmos. Chem.*  
741 *Phys.*, 13, 6647-6662, 10.5194/acp-13-6647-2013, 2013.

742 IPCC: Climate Change 2013, The Physical Science Basis, Cambridge University Press,  
743 Cambridge, United Kingdom and New York, NY, USA, 2013.

744 Jain, A., Yang, G., and Yalkowsky, S. H.: Estimation of melting points of organic  
745 compounds, *Ind. Eng. Chem. Res.*, 43, 7618-7621, 10.1021/ie049378m, 2004.

746 Jain, A., and Yalkowsky, S. H.: Estimation of melting points of organic compounds-II, *J.*  
747 *Pharm. Sci.*, 95, 2562-2618, 10.1002/jps.20634, 2006.

748 Jensen, E. J., Smith, J. B., Pfister, L., Pittman, J. V., Weinstock, E. M., Sayres, D. S., Herman,  
749 R. L., Troy, R. F., Rosenlof, K., Thompson, T. L., Fridlind, A. M., Hudson, P. K., Cziczo, D.  
750 J., Heymsfield, A. J., Schmitt, C., and Wilson, J. C.: Ice supersaturations exceeding 100% at  
751 the cold tropical tropopause: implications for cirrus formation and dehydration, *Atmos. Chem.*  
752 *Phys.*, 5, 851-862, 2005.

753 Kalberer, M., Paulsen, D., Sax, M., Steinbacher, M., Dommen, J., Prevot, A. S. H., Fisseha,  
754 R., Weingartner, E., Frankevich, V., Zenobi, R., and Baltensperger, U.: Identification of  
755 polymers as major components of atmospheric organic aerosols, *Science*, 303, 1659-1662,  
756 2004.

757 Kautzman, K. E., Surratt, J. D., Chan, M. N., Chan, A. W. H., Hersey, S. P., Chhabra, P. S.,  
758 Dalleska, N. F., Wennberg, P. O., Flagan, R. C., and Seinfeld, J. H.: Chemical Composition of  
759 Gas- and Aerosol-Phase Products from the Photooxidation of Naphthalene, *J. Phys. Chem. A*,  
760 114, 913-934, 10.1021/jp908530s, 2010.

761 Kidd, C., Perraud, V., Wingen, L. M., and Finlayson-Pitts, B. J.: Integrating phase and  
762 composition of secondary organic aerosol from the ozonolysis of  $\alpha$ -pinene, *Proc. Natl. Acad.*  
763 *Sci. USA*, 10.1073/pnas.1322558111, 2014.

764 Knopf, D. A., Wang, B., Laskin, A., Moffet, R. C., and Gilles, M. K.: Heterogeneous  
765 nucleation of ice on anthropogenic organic particles collected in Mexico City, *Geophys. Res.*  
766 *Lett.*, 37, L11803, 10.1029/2010gl043362, 2010.

767 Knopf, D. A., Alpert, P. A., Wang, B., O'Brien, R. E., Kelly, S. T., Laskin, A., Gilles, M. K.,  
768 and Moffet, R. C.: Microspectroscopic imaging and characterization of individually identified  
769 ice nucleating particles from a case field study, *J. Geophys. Res. Atmos.*, 119, JD021866,  
770 2014.

771 Koop, T., Luo, B. P., Tsias, A., and Peter, T.: Water activity as the determinant for  
772 homogeneous ice nucleation in aqueous solutions, *Nature*, 406, 611-614, 10.1038/35020537,  
773 2000.

774 Koop, T., Bookhold, J., Shiraiwa, M., and Pöschl, U.: Glass transition and phase state of  
775 organic compounds: dependency on molecular properties and implications for secondary  
776 organic aerosols in the atmosphere, *Phys. Chem. Chem. Phys.*, 13, 19238-19255, 2011.

777 Kuwata, M., and Martin, S. T.: Phase of atmospheric secondary organic material affects its  
778 reactivity, *Proc. Natl. Acad. Sci. USA*, 109, 17354-17359, 10.1073/pnas.1209071109, 2012.

779 Lambe, A. T., Onasch, T. B., Massoli, P., Croasdale, D. R., Wright, J. P., Ahern, A. T.,  
780 Williams, L. R., Worsnop, D. R., Brune, W. H., and Davidovits, P.: Laboratory studies of the  
781 chemical composition and cloud condensation nuclei (CCN) activity of secondary organic  
782 aerosol (SOA) and oxidized primary organic aerosol (OPOA), *Atmos. Chem. Phys.*, 11, 8913-  
783 8928, 10.5194/acp-11-8913-2011, 2011.

784 Lide, D. R.: *CRC Handbook of Chemistry and Physics*, CRC Press, National Institute of  
785 Standards and Technology, Boca Raton, FL, 2005.

786 Lienhard, D. M., Bones, D. L., Zuend, A., Krieger, U. K., Reid, J. P., and Peter, T.:  
787 Measurements of Thermodynamic and Optical Properties of Selected Aqueous Organic and  
788 Organic-Inorganic Mixtures of Atmospheric Relevance, *J. Phys. Chem. A*, 116, 9954-9968,  
789 10.1021/jp3055872, 2012.

790 Lienhard, D. M., Huisman, A. J., Bones, D. L., Te, Y. F., Luo, B. P., Krieger, U. K., and Reid,  
791 J. P.: Retrieving the translational diffusion coefficient of water from experiments on single  
792 levitated aerosol droplets, *Phys. Chem. Chem. Phys.*, 16, 16677-16683, 10.1039/c4cp01939c,  
793 2014.

794 Marcolli, C.: Deposition nucleation viewed as homogeneous or immersion freezing in pores  
795 and cavities, *Atmos. Chem. Phys.*, 14, 2071-2104, 10.5194/acp-14-2071-2014, 2014.

796 Mikhailov, E., Vlasenko, S., Martin, S. T., Koop, T., and Pöschl, U.: Amorphous and  
797 crystalline aerosol particles interacting with water vapor: conceptual framework and  
798 experimental evidence for restructuring, phase transitions and kinetic limitations, *Atmos.*  
799 *Chem. Phys.*, 9, 9491-9522, 2009.

800 Murray, B. J., Wilson, T. W., Dobbie, S., Cui, Z. Q., Al-Jumur, S., Mohler, O., Schnaiter, M.,  
801 Wagner, R., Benz, S., Niemand, M., Saathoff, H., Ebert, V., Wagner, S., and Karcher, B.:  
802 Heterogeneous nucleation of ice particles on glassy aerosols under cirrus conditions, *Nature*  
803 *Geosci.*, 3, 233-237, 10.1038/ngeo817, 2010.

804 O'Meara, S., Booth, A. M., Barley, M. H., Topping, D., and McFiggans, G.: An assessment of  
805 vapour pressure estimation methods, *Phys. Chem. Chem. Phys.*, 16, 19453-19469,  
806 10.1039/c4cp00857j, 2014.

807 Perraud, V., Bruns, E. A., Ezell, M. J., Johnson, S. N., Yu, Y., Alexander, M. L., Zelenyuk,  
808 A., Imre, D., Chang, W. L., Dabdub, D., Pankow, J. F., and Finlayson-Pitts, B. J.:  
809 Nonequilibrium atmospheric secondary organic aerosol formation and growth, *Proc. Natl.*  
810 *Acad. Sci. USA*, 109, 2836-2841, 10.1073/pnas.1119909109, 2012.

811 Petters, M. D., and Kreidenweis, S. M.: A single parameter representation of hygroscopic  
812 growth and cloud condensation nucleus activity, *Atmos. Chem. Phys.*, 7, 1961-1971, 2007.

813 Price, H. C., Murray, B. J., Mattsson, J., O'Sullivan, D., Wilson, T. W., Baustian, K. J., and  
814 Benning, L. G.: Quantifying water diffusion in high-viscosity and glassy aqueous solutions  
815 using a Raman isotope tracer method, *Atmos. Chem. Phys.*, 14, 3817-3830, 10.5194/acp-14-  
816 3817-2014, 2014.

817 Pruppacher, H., and Klett, J.: *Microphysics of clouds and precipitation*, 2 ed., Kluwer  
818 Academic Publishers, Boston, MA, 1997.

819 Rampp, M., Buttersack, C., and Ludemann, H. D.:  $c,T$ -dependence of the viscosity and the  
820 self-diffusion coefficients in some aqueous carbohydrate solutions, *Carbohydr. Res.*, 328, 561-  
821 572, 2000.

822 Renbaum-Wolff, L., Grayson, J. W., Bateman, A. P., Kuwata, K., Sellier, M., Murray, B. J.,  
823 Schilling, J. E., Martin, S. T., and Bertram, A. K.: Viscosity of  $\alpha$ -pinene secondary organic  
824 material and implications for particle growth and reactivity, *Proc. Natl. Acad. Sci. USA*, 110,  
825 8014-8019, 10.1073/pnas.1219548110 2013.

826 Rickards, A. M. J., Miles, R. E. H., Davies, J. F., Marshall, F. H., and Reid, J. P.:  
827 Measurements of the Sensitivity of Aerosol Hygroscopicity and the kappa Parameter to the  
828 O/C Ratio, *J. Phys. Chem. A*, 117, 14120-14131, 10.1021/jp407991n, 2013.

829 Saukko, E., Lambe, A. T., Massoli, P., Koop, T., Wright, J. P., Croasdale, D. R., Pedernera,  
830 D. A., Onasch, T. B., Laaksonen, A., Davidovits, P., Worsnop, D. R., and Virtanen, A.:  
831 Humidity-dependent phase state of SOA particles from biogenic and anthropogenic  
832 precursors, *Atmos. Chem. Phys.*, 12, 7517-7529, 10.5194/acp-12-7517-2012, 2012.

833 Schill, G. P., and Tolbert, M. A.: Heterogeneous ice nucleation on phase-separated organic-  
834 sulfate particles: effect of liquid vs. glassy coatings, *Atmos. Chem. Phys.*, 13, 4681-4695,  
835 10.5194/acp-13-4681-2013, 2013.

836 Schill, G. P., De Haan, D. O., and Tolbert, M. A.: Heterogeneous Ice Nucleation on Simulated  
837 Secondary Organic Aerosol, *Environ. Sci. Technol.*, 48, 1675-1682, 10.1021/es4046428,  
838 2014.

839 Shilling, J. E., Chen, Q., King, S. M., Rosenoern, T., Kroll, J. H., Worsnop, D. R., DeCarlo,  
840 P. F., Aiken, A. C., Sueper, D., Jimenez, J. L., and Martin, S. T.: Loading-dependent  
841 elemental composition of alpha-pinene SOA particles, *Atmos. Chem. Phys.*, 9, 771-782,  
842 2009.

843 Shiraiwa, M., Ammann, M., Koop, T., and Pöschl, U.: Gas uptake and chemical aging of  
844 semisolid organic aerosol particles, *Proc. Natl. Acad. Sci. USA*, 108, 11003-11008,  
845 10.1073/pnas.1103045108, 2011.

846 Shiraiwa, M., Pfrang, C., Koop, T., and Pöschl, U.: Kinetic multi-layer model of gas-particle  
847 interactions in aerosols and clouds (KM-GAP): linking condensation, evaporation and  
848 chemical reactions of organics, oxidants and water, *Atmos. Chem. Phys.*, 12, 2777-2794,  
849 10.5194/acp-12-2777-2012, 2012.

850 Shiraiwa, M., Yee, L. D., Schilling, K. A., Loza, C. L., Craven, J. S., Zuend, A., Ziemann, P.  
851 J., and Seinfeld, J. H.: Size distribution dynamics reveal particle-phase chemistry in organic  
852 aerosol formation, *Proc. Natl. Acad. Sci. USA*, 110, 11746-11750, 10.1073/pnas.1307501110,  
853 2013a.

854 Shiraiwa, M., Zuend, A., Bertram, A. K., and Seinfeld, J. H.: Gas-particle partitioning of  
855 atmospheric aerosols: interplay of physical state, non-ideal mixing and morphology, *Phys.*  
856 *Chem. Chem. Phys.*, 15, 11441-11453, 10.1039/C3CP51595H, 2013b.

857 Song, M., Marcolli, C., Krieger, U. K., Zuend, A., and Peter, T.: Liquid-liquid phase  
858 separation and morphology of internally mixed dicarboxylic acids/ammonium sulfate/water  
859 particles, *Atmos. Chem. Phys.*, 12, 2691-2712, 10.5194/acp-12-2691-2012, 2012.

860 Surratt, J. D., Murphy, S. M., Kroll, J. H., Ng, N. L., Hildebrandt, L., Sorooshian, A.,  
861 Szmigielski, R., Vermeylen, R., Maenhaut, W., Claeys, M., Flagan, R. C., and Seinfeld, J. H.:  
862 Chemical composition of secondary organic aerosol formed from the photooxidation of  
863 isoprene, *J. Phys. Chem. A*, 110, 9665-9690, 10.1021/jp061734m, 2006.

864 Szmigielski, R., Surratt, J. D., Gomez-Gonzalez, Y., Van der Veken, P., Kourtchev, I.,  
865 Vermeylen, R., Blockhuys, F., Jaoui, M., Kleindienst, T. E., Lewandowski, M., Offenberg, J.  
866 H., Edney, E. O., Seinfeld, J. H., Maenhaut, W., and Claeys, M.: 3-methyl-1,2,3-  
867 butanetricarboxylic acid: An atmospheric tracer for terpene secondary organic aerosol,  
868 *Geophys. Res. Lett.*, 34, 6, 10.1029/2007gl031338, 2007.

869 Tammann, G., and Hesse, W.: The dependency of viscosity on temperature in hypothermic  
870 liquids, *Z. Anorg. Allg. Chem.*, 156, 14, 1926.

871 Tong, H. J., Reid, J. P., Bones, D. L., Luo, B. P., and Krieger, U. K.: Measurements of the  
872 timescales for the mass transfer of water in glassy aerosol at low relative humidity and  
873 ambient temperature, *Atmos. Chem. Phys.*, 11, 4739-4754, 10.5194/acp-11-4739-2011, 2011.

874 Vaden, T. D., Imre, D., Beranek, J., Shrivastava, M., and Zelenyuk, A.: Evaporation kinetics  
875 and phase of laboratory and ambient secondary organic aerosol, *Proc. Natl. Acad. Sci. USA*,  
876 108, 2190-2195, 10.1073/pnas.1013391108, 2011.

877 Virtanen, A., Joutsensaari, J., Koop, T., Kannosto, J., YliPirilä, P., Leskinen, J., Mäkelä, J.  
878 M., Holopainen, J. K., Pöschl, U., Kulmala, M., Worsnop, D. R., and Laaksonen, A.: An  
879 amorphous solid state of biogenic secondary organic aerosol particles, *Nature*, 467, 824-827,  
880 doi:10.1038/nature09455, 2010.

881 Vogel, H.: The temperature dependence law of the viscosity of fluids, *Physik. Z.*, 22, 645-  
882 646, 1921.

883 Wagner, R., Mohler, O., Saathoff, H., Schnaiter, M., Skrotzki, J., Leisner, T., Wilson, T. W.,  
884 Malkin, T. L., and Murray, B. J.: Ice cloud processing of ultra-viscous/glassy aerosol particles  
885 leads to enhanced ice nucleation ability, *Atmos. Chem. Phys.*, 12, 8589-8610, 10.5194/acp-  
886 12-8589-2012, 2012.

887 Wang, B. B., Lambe, A. T., Massoli, P., Onasch, T. B., Davidovits, P., Worsnop, D. R., and  
888 Knopf, D. A.: The deposition ice nucleation and immersion freezing potential of amorphous  
889 secondary organic aerosol: Pathways for ice and mixed-phase cloud formation, *J. Geophys.*  
890 *Res. Atmos.*, 117, D16209, 10.1029/2012jd018063, 2012.

891 Wilson, T. W., Murray, B. J., Wagner, R., Mohler, O., Saathoff, H., Schnaiter, M., Skrotzki,  
892 J., Price, H. C., Malkin, T. L., Dobbie, S., and Al-Jumur, S.: Glassy aerosols with a range of  
893 compositions nucleate ice heterogeneously at cirrus temperatures, *Atmos. Chem. Phys.*, 12,  
894 8611-8632, 10.5194/acp-12-8611-2012, 2012.

895 Yee, L. D., Craven, J. S., Loza, C. L., Schilling, K. A., Ng, N. L., Canagaratna, M. R.,  
896 Ziemann, P. J., Flagan, R. C., and Seinfeld, J. H.: Secondary organic aerosol formation from  
897 low-NO<sub>x</sub> photooxidation of dodecane: evolution of multigeneration gas-phase chemistry and  
898 aerosol composition, *J. Phys. Chem. A*, 116, 6211-6230, 2012.

899 You, Y., Renbaum-Wolff, L., Carreras-Sospedra, M., Hanna, S. J., Hiranuma, N., Kamal, S.,  
900 Smith, M. L., Zhang, X. L., Weber, R. J., Shilling, J. E., Dabdub, D., Martin, S. T., and  
901 Bertram, A. K.: Images reveal that atmospheric particles can undergo liquid-liquid phase  
902 separations, *Proc. Natl. Acad. Sci. USA*, 109, 13188-13193, 10.1073/pnas.1206414109, 2012.

903 You, Y., Smith, M. L., Song, M. J., Martin, S. T., and Bertram, A. K.: Liquid-liquid phase  
904 separation in atmospherically relevant particles consisting of organic species and inorganic  
905 salts, *International Reviews in Physical Chemistry*, 33, 43-77,  
906 10.1080/0144235x.2014.890786, 2014.

907 Yu, H., Kaufman, Y. J., Chin, M., Feingold, G., Remer, L. A., Anderson, T. L., Balkanski, Y.,  
908 Bellouin, N., Boucher, O., Christopher, S., DeCola, P., Kahn, R., Koch, D., Loeb, N., Reddy,  
909 M. S., Schulz, M., Takemura, T., and Zhou, M.: A review of measurement-based assessments  
910 of the aerosol direct radiative effect and forcing, *Atmos. Chem. Phys.*, 6, 613-666, 2006.

911 Zhang, X., Schwantes, R. H., Coggon, M. M., Loza, C. L., Schilling, K. A., Flagan, R. C., and  
912 Seinfeld, J. H.: Role of ozone in SOA formation from alkane photooxidation, *Atmos. Chem.*  
913 *Phys.*, 14, 1733-1753, 10.5194/acp-14-1733-2014, 2014.

914 Zhou, S., Shiraiwa, M., McWhinney, R., Pöschl, U., and Abbatt, J. P. D.: Kinetic limitations  
915 in gas-particle reactions arising from slow diffusion in secondary organic aerosol, *Faraday*  
916 *Discuss.*, 165, 391-406, 10.1039/C3FD00030C, 2013.

917 Zobrist, B., Weers, U., and Koop, T.: Ice nucleation in aqueous solutions of poly ethylene  
918 glycol with different molar mass, *J. Chem. Phys.*, 118, 10254-10261, 10.1063/1.1571818,  
919 2003.

920 Zobrist, B., Marcolli, C., Pedernera, D. A., and Koop, T.: Do atmospheric aerosols form  
921 glasses?, *Atmos. Chem. Phys.*, 8, 5221-5244, 2008.

922 Zobrist, B., Soonsin, V., Luo, B. P., Krieger, U. K., Marcolli, C., Peter, T., and Koop, T.:  
923 Ultra-slow water diffusion in aqueous sucrose glasses, *Phys. Chem. Chem. Phys.*, 13, 3514-  
924 3526, 10.1039/c0cp01273d, 2011.

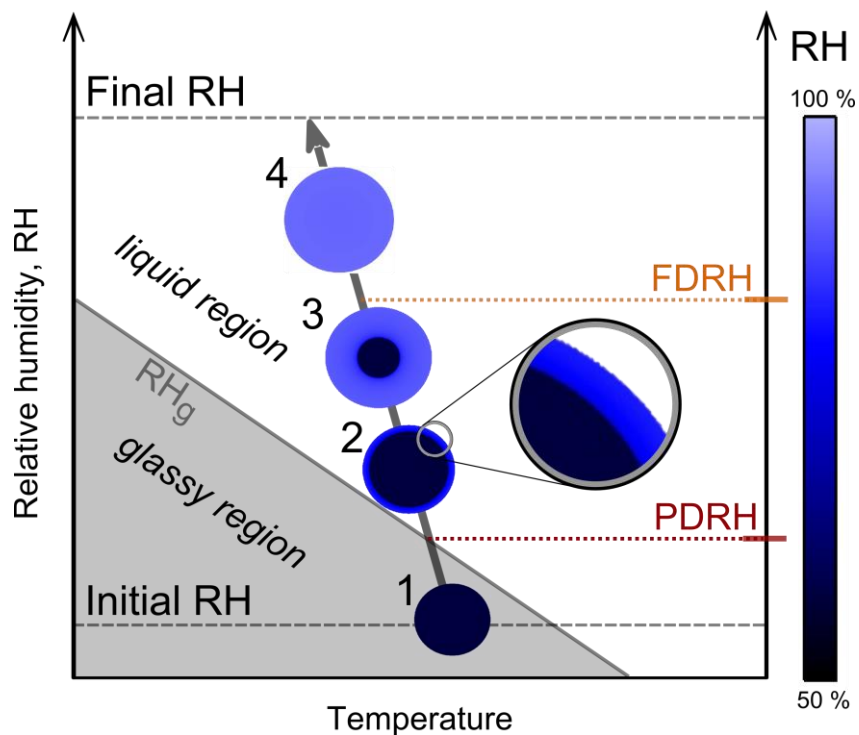
925 Zuend, A., and Seinfeld, J. H.: Modeling the gas-particle partitioning of secondary organic  
926 aerosol: the importance of liquid-liquid phase separation, *Atmos. Chem. Phys.*, 12, 3857-  
927 3882, 10.5194/acp-12-3857-2012, 2012.

928

929 Table A1. Assumed physical properties of SOA classes for use in conjunction with diffusivity  
 930 estimation scheme.

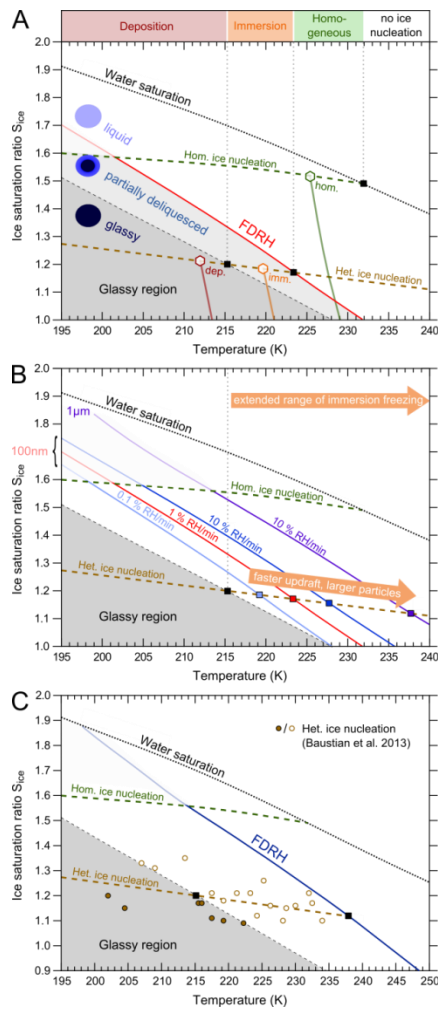
SOA Class	O/C	$T_{g,org}$ (K)	$k_{GT}$	$\kappa_{org}$
A-PINENE	0.3	$228.9 \pm 10.6$	2.5	$0.084 \pm 0.012$
	0.5	$278.5 \pm 7.0$	2.5	$0.120 \pm 0.020$
	0.7	$328.1 \pm 12.8$	2.5	$0.156 \pm 0.028$
ISOPRENE	0.6	$258.2 \pm 22.2$	2.5	$0.138 \pm 0.024$
	0.8	$287.2 \pm 11.9$	2.5	$0.174 \pm 0.032$
	1.0	$316.3 \pm 19.1$	2.5	$0.210 \pm 0.040$
NAPHTHALENE	0.3	$294.2 \pm 5.7$	2.5	$0.084 \pm 0.012$
	0.5	$313.1 \pm 8.8$	2.5	$0.120 \pm 0.020$
	0.7	$332.0 \pm 15.0$	2.5	$0.156 \pm 0.028$
DODECANE	0.1	$210.3 \pm 9.7$	2.5	$0.048 \pm 0.004$
	0.3	$216.8 \pm 5.1$	2.5	$0.084 \pm 0.012$
	0.5	$223.4 \pm 11.4$	2.5	$0.120 \pm 0.020$
KOOP SOA	---	$270 \pm 21$	$2.5 \pm 1$	$0.1008^{+0.1008}$ $-0.0504$

931



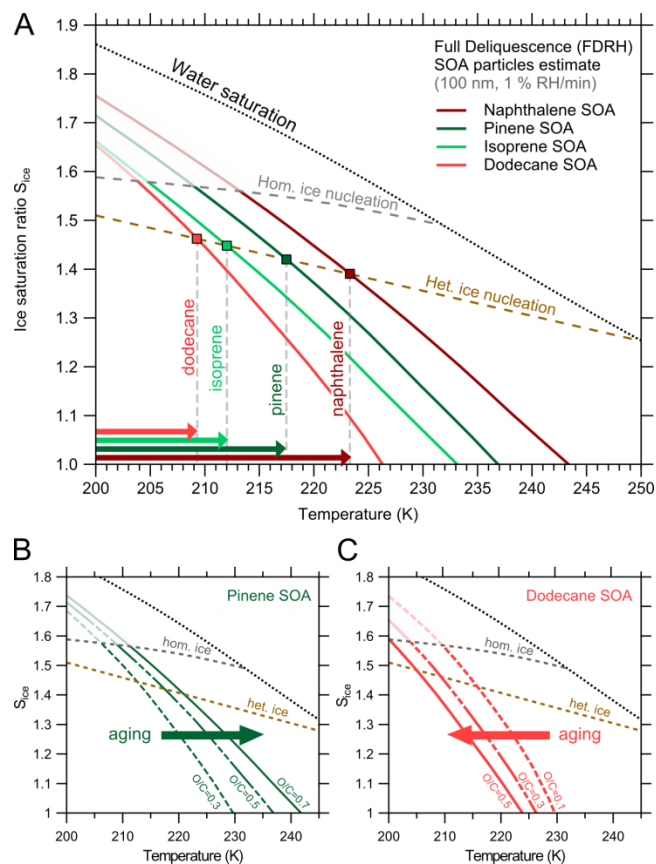
932

933 Figure 1. Schematic temporal evolution of particle morphology along a trajectory of an  
 934 atmospheric updraft (grey arrow). Humidification of ambient air upon adiabatic expansion  
 935 leads to liquefaction of initially glassy particles (dark blue color, 1) via core-shell  
 936 morphologies (2, 3) to liquid particles (light blue color, 4). Whereas partial deliquescence  
 937 (PDRH) coincides with  $RH_g$ , full deliquescence (FDRH) is delayed to much higher RH,  
 938 indicating that diffusion processes occur on much longer time scales than humidification. The  
 939 speed of the displayed trajectory corresponds to that typical for cloud chamber or  
 940 environmental cell experiments ( $0.1 - 1.5 \text{ K min}^{-1}$ ,  $1 - 15 \text{ \% RH min}^{-1}$ ).



941

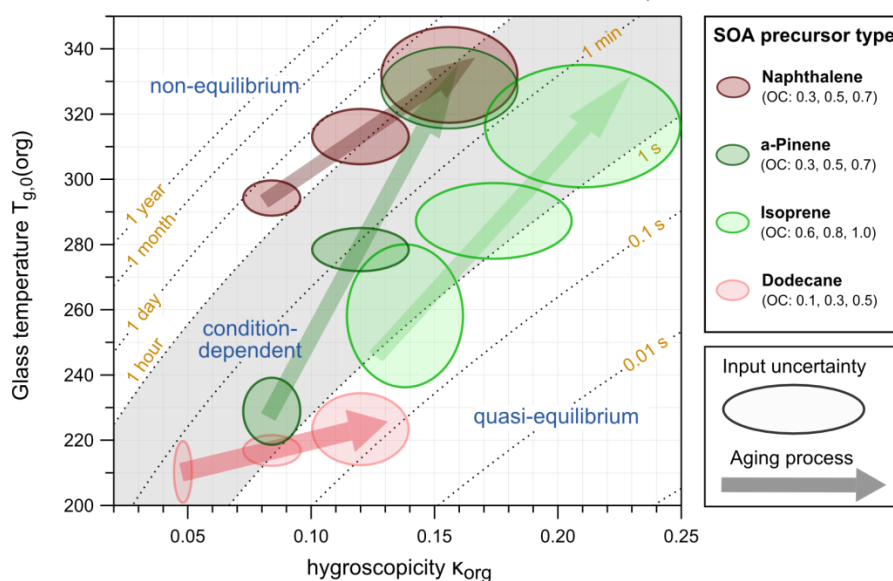
942 Figure 2. (A) Simulated regimes of heterogeneous and homogeneous ice nucleation in the  
 943 humidification of sucrose particles. The red solid line indicates full deliquescence relative  
 944 humidities (FDRH) for 100 nm particles exposed to a humidification rate of 1 % RH min<sup>-1</sup> ( $\approx$   
 945 0.2 m s<sup>-1</sup> atmospheric updraft). Example trajectories start at ice saturation, follow a constant  
 946 dew point line and end at expected ice nucleation (hexagonal markers) with deposition (red),  
 947 immersion (orange), and homogeneous (green) freezing. (B) Effects of different particles  
 948 sizes and humidification rates on FDRH. The upper boundary for immersion freezing is  
 949 extended to high temperatures for large particle radii and high humidification rates and is  
 950 expected to occur up to 238 K for the most extreme scenario (1  $\mu\text{m}$ , 10 % RH min<sup>-1</sup>, purple  
 951 solid line). (C) Application to the experimental conditions in Baustian et al. (2013), i.e. 4  $\mu\text{m}$   
 952 particles humidified at a rate of 1 % RH min<sup>-1</sup>, leads to FDRH that is able to explain all  
 953 observed experimental ice onsets (brown circles). The thermodynamic glass transition divides  
 954 the experimental data in events of deposition ice nucleation (closed circles) and immersion  
 955 freezing (open circles).



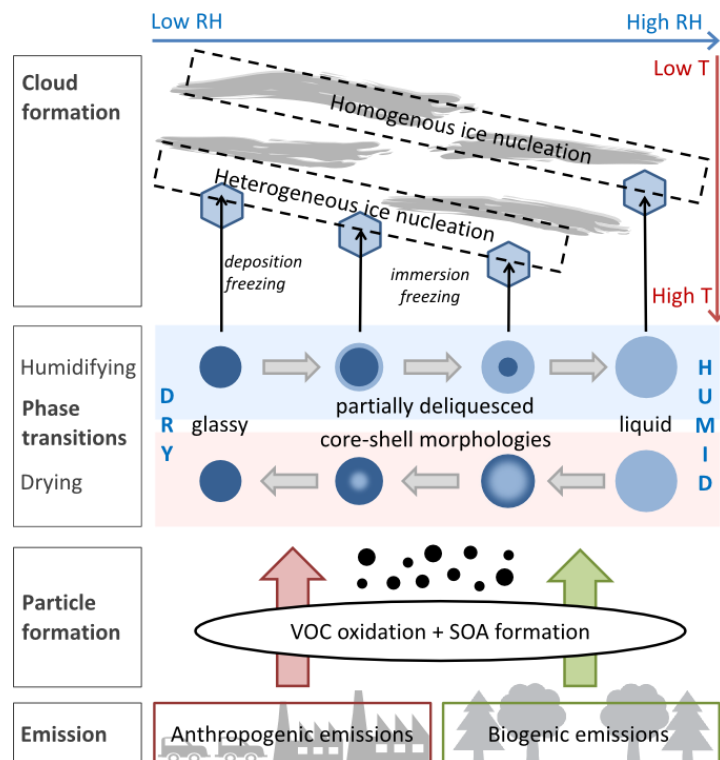
956

957 Figure 3. (A) Simulated humidification of SOA particles from the four different precursors a-  
 958 pinene, isoprene, dodecane and naphthalene. Naphthalene SOA (dark red) shows the latest  
 959 deliquescence, whereas dodecane SOA (light red) liquefied rather early in the simulations.  
 960 The two biogenic SOA estimates lie between both extremes with pinene SOA (dark green)  
 961 showing slightly later deliquescence than isoprene SOA. Intercepts (square markers) with a  
 962 heterogeneous nucleation onset typical for SOA (brown dashed line) indicate upper  
 963 temperature limits for immersion freezing (arrows on x-axis). The effect of particle ageing  
 964 also depends on precursor type: Pinene SOA (B) shows hardening upon increase in O/C  
 965 (indicated by higher FDRH), whereas dodecane SOA (C) exhibits softening (indicated by  
 966 lower FDRH). Similarly, isoprene and naphthalene SOA show only moderate hardening and  
 967 softening, respectively (Fig. S5).

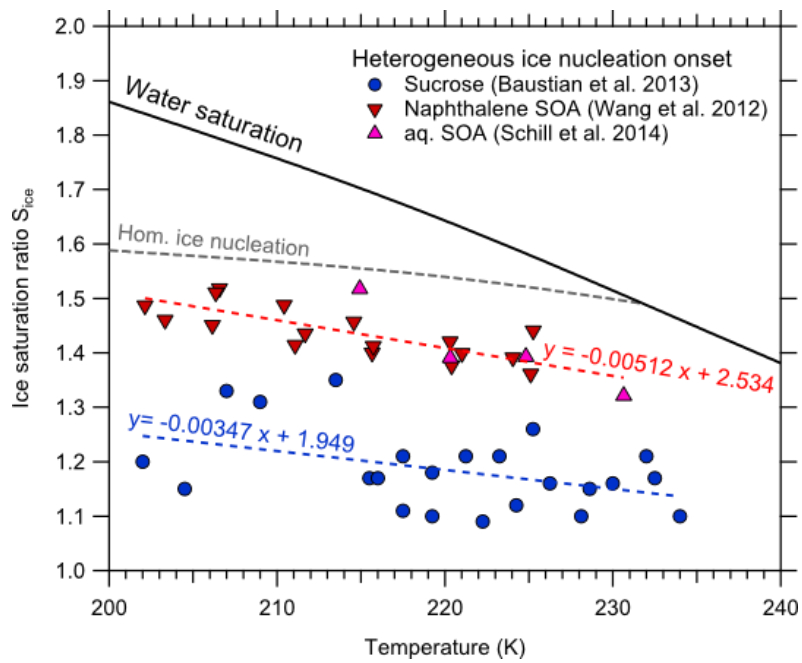
Water diffusion time scales in SOA (220 K,  $S_{ice} = 1.45$ ,  $d_p = 100$  nm)



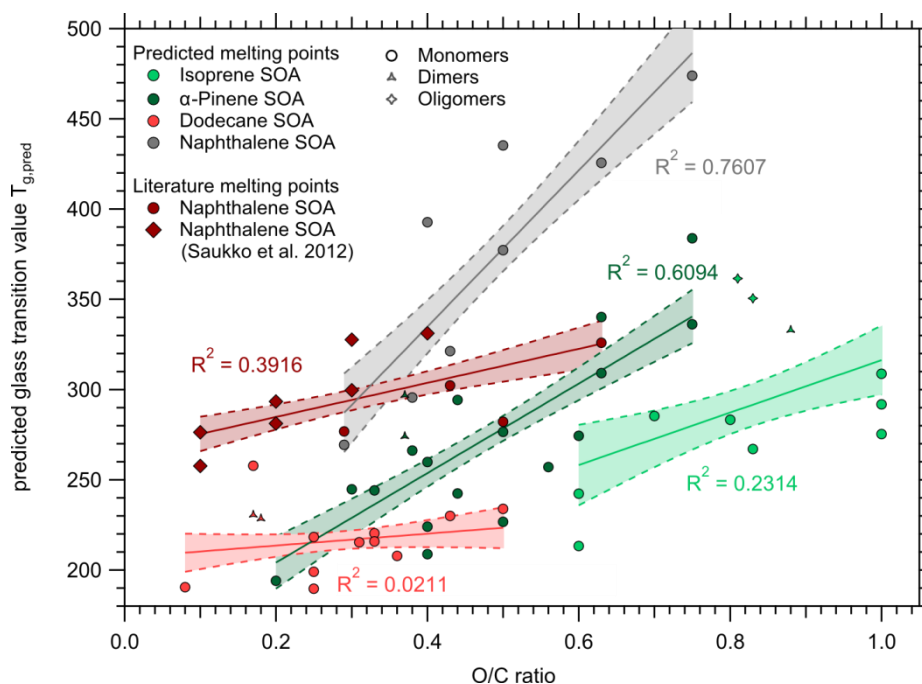
968  
 969 Figure 4. Characteristic time scales of water diffusion in SOA as function of hygroscopicity  
 970  $\kappa_{org}$  and glass transition temperatures of the pure organic matrix  $T_{g,org}$ . Calculations have been  
 971 performed at 220 K,  $S_{ice} = 1.45$  and for 100 nm particles. Oval shapes confine estimated  
 972 ranges in  $\kappa_{org}$  and  $T_{g,org}$  for the four SOA types in three different oxidation states (Appendix A  
 973 and Table A1). The grey area indicates the time scale of typical atmospheric updrafts (1 s to 1  
 974 h) and thus divides the plot in areas of quasi-equilibrium and non-equilibrium water diffusion.  
 975 Within the grey area, the relative speed of both processes depends upon the actual  
 976 atmospheric conditions. The aging process is indicated by arrows pointing from regions of  
 977 low O/C to regions of high O/C.



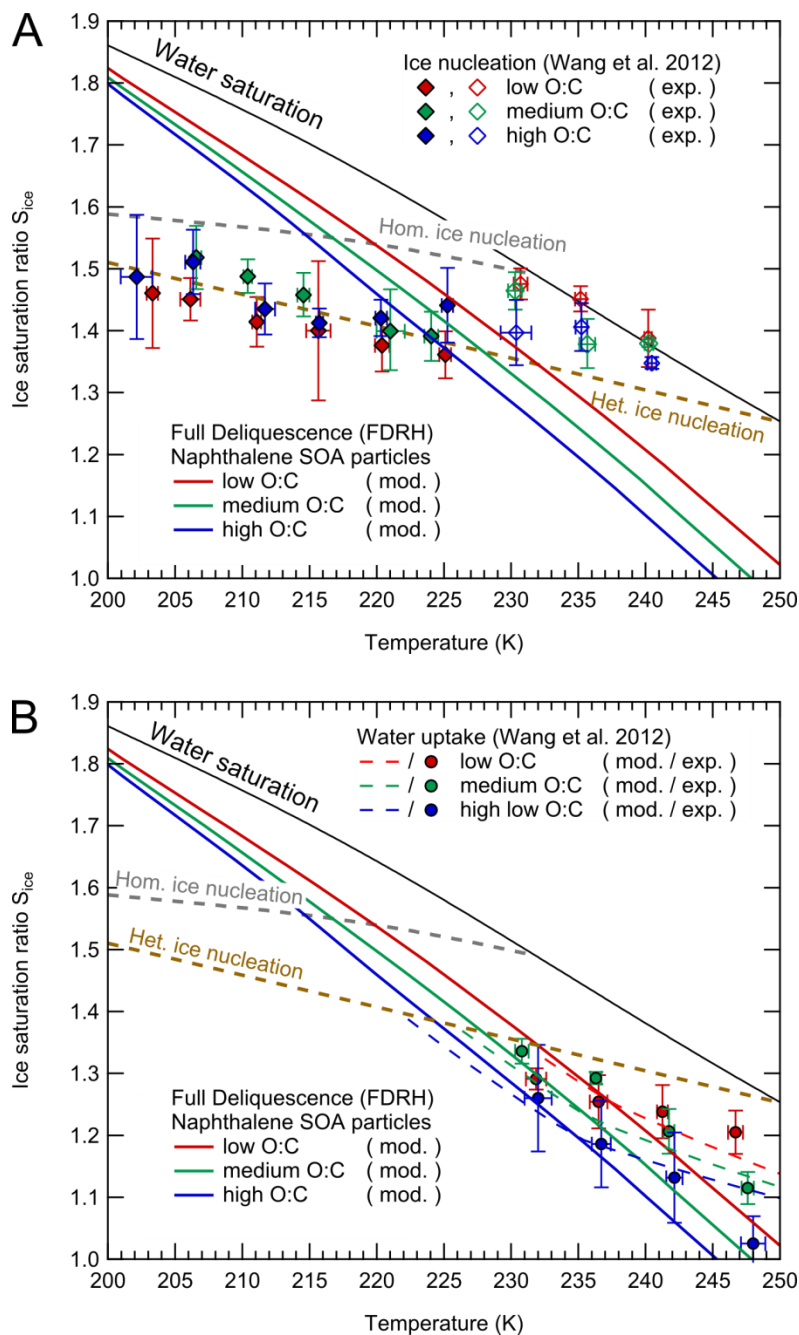
1  
 2 Figure 5. Overview of processes in organic aerosol particles affecting atmospheric cloud  
 3 formation. Particles form by oxidation of volatile organic compounds (VOCs) originating  
 4 from anthropogenic and biogenic emissions. The dominating cloud formation process  
 5 depends on particle phase state, which is a function of temperature and humidity. Humidity-  
 6 induced phase transitions between phase states may be kinetically limited and occur under  
 7 formation of partially deliquesced particles with core-shell morphologies. Glassy or partially  
 8 deliquesced particles are able to undergo heterogeneous ice nucleation, occurring at lower  
 9 relative humidity or higher temperature than homogeneous ice nucleation of liquid particles.



1  
 2 Figure A1. Determination of heterogeneous ice nucleation onsets. For sucrose, data from  
 3 Baustian et al. (2013) (blue circles) are fitted. For SOA, deposition freezing data on  
 4 Naphthalene SOA from Wang et al. (2012) (red downward triangles) as well as nucleation  
 5 data on aqSOA from Schill et al. (2014) (pink upward triangles) are used. The resulting linear  
 6 regression fits (blue and red dashed lines) lie significantly below the homogeneous nucleation  
 7 limit and are displayed along with their parameterizations.

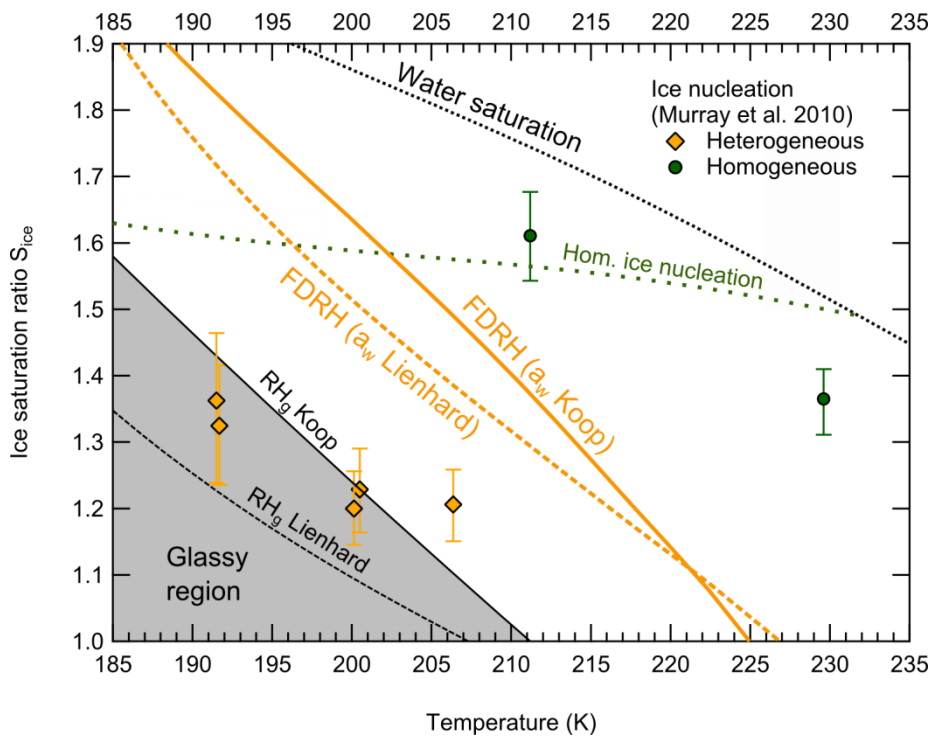


1  
 2 Figure A2. Predicted glass transition values of SOA marker substances as function of O/C  
 3 ratio. The predicted  $T_{g,org}$  exhibit a linear correlation with O/C for each of the four SOA  
 4 systems. Solid lines are robust linear regressions using a bisquare weighting function and  
 5 shaded areas are confidence intervals at the  $1\sigma$  level. Anthropogenic aliphatic SOA  
 6 constituents show the lowest values of  $T_{g,org}$  and a weak dependence on O/C. In contrast,  
 7 aromatic SOA shows the highest glass transition values despite a rather low average O/C  
 8 ratio.



1

2 Figure B1. Comparison between calculation results of naphthalene SOA deliquescence and  
 3 experimental ice nucleation and water uptake data from Wang et al. (2012). For the numerical  
 4 simulations, aerosol particles are assumed to be 1  $\mu\text{m}$  in diameter and are humidified at a rate  
 5 of 1 %  $\text{RH min}^{-1}$ , corresponding to a cooling rate of about 0.1  $\text{K min}^{-1}$  used by Wang et al.



1

2 Figure B2. Comparison between calculation results of citric acid aerosol deliquescence  
 3 (orange lines) and experimental ice nucleation data from Murray et al. (2010) (orange  
 4 diamonds, green circles). In the numerical simulations, 150 nm diameter aerosol particles are  
 5 humidified at a rate of 12 % RH min<sup>-1</sup>, corresponding to a cooling rate around 1-2 K min<sup>-1</sup>  
 6 typical for cloud chamber experiments. Black lines and shaded areas confine the region where  
 7 a glass is the favored thermodynamic state. The dashed lines were obtained using the water  
 8 activity parameterization provided by Lienhard et al. (2012), whereas the solid lines were  
 9 obtained with the parameterization in Koop et al. (2011).